IEEE Access
Multidisciplinary | Rapid Review | Open Access Journal

Received February 12, 2019, accepted February 25, 2019, date of publication March 5, 2019, date of current version March 20, 2019.

Digital Object Identifier 10.1109/ACCESS.2019.2903185

A Novel Doppler Rate Estimator Based on Fractional Fourier Transform for High-Dynamic GNSS Signal

YIRAN LUO[1,2,3], CHUNYANG YU[3], SHAOHUA CHEN[3], JIAN LI[1,2], HANG RUAN[4], AND NASER EL-SHEIMY[3]

[1]Radar Research Laboratory, School of Information and Electronics, Beijing Institute of Technology, Beijing 100081, China
[2]Key Laboratory of Electronic and Information Technology in Satellite Navigation, Ministry of Education, Beijing Institute of Technology, Beijing 100081, China
[3]Department of Geomatics Engineering, University of Calgary, Calgary T2N1N4, Canada
[4]Beijing Institute of Radio Measurement, Beijing 100854, China

Corresponding author: Chunyang Yu (chunyang.yu@ucalgary.ca)

This work was supported in part by the National Natural Science Foundation of China under Grant 31727901, and in part by the Chang Jiang Scholars Programme under Grant T2012122.

ABSTRACT When the fractional Fourier transform (FRFT) is introduced into the weak and high-dynamic global navigation satellite system (GNSS) signal acquisition, the 2-D search cell will be transferred to a 3-D one with respect to the code chip, the Doppler shift, and the Doppler rate. The proper determinations of the code bin and Doppler shift bin in the acquisition process have already been covered in the previous researches. The aim of this paper is to provide an exhaustive analysis of the approach to specify an optimal FRFT order bin, in terms of the Doppler shift rate. The lower and upper bound of FRFT order ranges is determined by the incoming signal dynamics. Then, we propose a precise model to yield an optimal FRFT order bin. Besides, a novel and fast Doppler estimator based on the non-linear least square (NLS) method is presented to improve the performance of the digital FRFT implementation. Finally, an alternate search procedure is proposed to reduce the singular estimations of the NLS method. The simulating examples demonstrate the performance of the proposed algorithms. It has been verified that the computation efficiency and the estimation accuracy have been significantly improved by proposed techniques.

INDEX TERMS Global navigation satellite system (GNSS) signal, linear frequency modulation (LFM), fractional Fourier transform (FRFT) order, acquisition, Doppler rate, non-linear least square (NLS).

I. INTRODUCTION

The deterioration of global navigation satellite system (GNSS) signal occurs through signal masking caused by foliage or building obstructions, ionospheric scintillation, multipath, jamming, and dynamics with respect to Doppler shift error or Doppler rate [1], [2]. Signal power loss can be unintentionally introduced in these situations, and the GNSS signal is hard to be acquired, or the receiver is easy to be out of lock from the tracking. To address the weak GNSS signal, longer coherent integration time is needed in acquisition and tracking. However, the receiver will be more sensitive to the accelerating incoming signal, clock oscillator vibration-induced noise, navigation bit sign transition and tracking-loop stability condition, when the long integration is adopted for the receiver design [3]. Vector tracking structures are proposed to mitigate the effect of the oscillator vibration-induced noise [4] and improve the tracking performance of high-dynamic carrier phase [5]; to solve the bit ambiguity, extending integration time coherently is reported by a high-sensitivity GNSS receiver design approach [3]; open-loop tracking method plays a significant role to implement a long coherent integration under a severe environment [6].

The GNSS receiver will undertake much dynamic stress under high dynamics that refers to many situations such as the missile navigation in military field [7], aerospace applications [8], and some deep space applications like moon missions [9]–[11] where the carrier-to-noise ratio density (C/N_0) is very low. Besides, if the inertial navigation system (INS) of the GNSS/INS integration system is influenced by the

The associate editor coordinating the review of this manuscript and approving it for publication was Venkata Ratnam Devanaboyina.

external interference at a high-dynamic situation, it may not work at all until the in-motion alignment is completed which will take a long time [12], [13]. Therefore, it is important to enhance the sensitivity of GNSS receiver as well as increase estimation accuracy of the initial Doppler for the weak signal processing performance in a high-dynamic environment.

Almeida proposed the physical definition of fractional Fourier transform (FRFT) that represents a rotation in the time domain [14]. The digital computation of the FRFT was published by Ozaktas *et al.* [15]. The FRFT was a widely used tool in radar [16]–[20], image processing [21], [22], communications [23], [24], in which the signal is formed with linear frequency modulation (LFM), and it is still currently a powerful tool for different applications [25]–[28].

The high-dynamic GNSS signal with Doppler rate is a typical LFM signal, so, it is reasonable to process dynamic GNSS signal with FRFT algorithm. The ordinary algorithms, e.g., serial-search acquisition and code-phase parallel-search acquisition, cannot well address weak and dynamic signals. Then, matched filter [29], [30] and partially matched filter [31] are introduced to design the high-sensitive GNSS receiver. However, the trade-off in terms of coherent integration time is hard to be made in a weak and high-dynamic environment. The fractional Fourier transform has been introduced to address the GNSS signal processing with linear frequency modulation in a weak and dynamic situation in recent times [32]–[34]. The computational complexity has been analyzed regardless of the effect of the FRFT order search rate [32]. The computational cost can largely be increased if an inappropriate order search rate, or FRFT order bin, is determined. The coarse-to-fine search strategy is widely used to decide an optimal FRFT order in the process of FRFT estimation as well [35], [36]. However, the extra implementations of the digital FRFT (DFRFT) should be considered to make decisions on a proper order bin. Fixed order bins are also decided by some experimental trials applied to the weak and dynamic GNSS signal acquisition [34]. However, the digital computational complexity will be highly increased due to a narrow FRFT order bin [15], [32]. Trade-off should be made on the estimation accuracy of the Doppler rate and FRFT order bin in the GNSS receiver design. There are few references that can provide a proper mathematical analysis to determine the proper FRFT order bin for different cases and the order bin will usually be reduced to a very small size to guarantee a high detection probability and a more accurate estimation for the Doppler rate in terms of the acquisition process of the high-dynamic GNSS signal. However, a very narrow order bin size will highly increase the computational complexity of the DFRFT implementation [32]. Hence, a fast DFRFT method is hard to be implemented due to this limitation.

Two purposes in terms of the acquisition of the high-dynamic GNSS signal can be achieved based on the DFRFT implementation by reducing the order bin size. At first, the detection probability of the acquisition process can be increased. Then, the estimation accuracy with respect to the Doppler rate can be improved. Since how to make a trade-off between the computational burden of the DFRFT and the detection probability of the weak and high-dynamic GNSS signal is not our contribution in this work, it might be done in the future work. Under this circumstance, we will mainly focus on how to improve the estimation accuracy of the Doppler rate for the LFM-based GNSS signal, and how to increase the computational efficiency of the DFRFT implementation in our research. A theoretical model with respect to the DFRFT amplitude [15] is proposed in this research. Two main contributions are made for the GNSS signal acquisition based on the FRFT algorithm in our work: Firstly, an approach to decide the optimal FRFT order bin is proposed; secondly, algorithms to largely improve the computation efficiency of the digital FRFT implementation for the Doppler rate estimation, i.e., a novel and fast Doppler rate estimator based on the DFRFT, is presented.

The organization for the remaining of this paper is provided as follows. Section II introduces the dynamic GNSS signal model based on linear frequency modulation; Section III contains a brief introduction about how the FRFT implementation works on the LFM-based GNSS signal, and a description related to the proposed theoretical model of the FRFT gain for the incoming GNSS signal; the way to compute an optimal FRFT order bin size with the proposed gain model is explained in Section IV; a detailed introduction for proposed Doppler rate estimator is provided in Section V; in Section VI, an overall flow chart for proposed three algorithms in this research is presented; the experimental results are included in the subsequent Section VII; Section VIII is devoted to some analysis and discussions corresponded to the simulation results; the last Section IX concludes this paper and presents its scope of the application in the future.

II. GNSS SIGNAL MODEL WITH LINEAR FREQUENCY MODULATION

The general form of the incoming intermediate frequency (IF) GNSS signal can be given by

$$s(t) = \sqrt{2P_r} D(t-\tau) C(t-\tau) \times \cos[2\pi (f_i + f_d) t + \varphi_0] + n(t) \quad (1)$$

where P_r is the power of the incoming signal; $D(\cdot)$ denotes the data code; $C(\cdot)$ stands for the spreading code; τ is the time delay of received signal; f_i, φ_0, and f_d represent the intermediate frequency, the initial carrier phase in radius, and Doppler of the incoming signal, respectively; $n(t)$ stands for the random noise. When the signal is transmitted in a high-dynamic environment, high-order components with respect to dynamics besides of Doppler shift should not be ignored in the received Doppler model of f_d. It is assumed that dynamics over quadratic terms with respect to the time variable will be not considered in our research. Under this circumstance, the high-dynamic GNSS signal is a typical type of LFM or chirp signal. The associated carrier phase in cycle

can be obtained as

$$\begin{aligned}\theta(t) &= \theta_0 - h\cdot\int_0^t (v+a\tau)\,d\tau \\ &= \theta_0 - hvt - \frac{1}{2}hat^2 \\ &= \theta_0 + f_0 t + \frac{1}{2}\mu t^2 \end{aligned} \tag{2}$$

with

$$f_0 = -hv, \quad \mu = -ha,\ h = \frac{f_r}{c} \tag{3}$$

where v is the line-of-sight (LOS) velocity between the satellite and the GNSS receiver antenna, a is the LOS acceleration, θ_0 denotes the initial carrier phase, f_0 is the initial Doppler shift, μ represents the Doppler shift rate, f_r and c represents the radio frequency of the received GNSS signal and the speed of light, respectively. Then, the highly dynamic signal model can be rewritten as

$$\begin{aligned}s(t) = &\sqrt{2P_r}D(t-\tau)\,C(t-\tau) \\ &\times\cos\left\{2\pi\,(f_i+f_0)\,t+\pi\mu t^2+2\pi\theta_0\right\}+n(t)\end{aligned} \tag{4}$$

Assuming that no bit transition error occurs during the integration process and bit sign ambiguity does not exist, after mixing with the local code and carrier replicas, the coherent integration outputs of the incoming signal in terms of in-phase (I) and quadrature (Q) components can be derived as

$$\begin{aligned}I(n) &= \sqrt{2P_r}R(\Delta\tau) \\ &\quad\times\int_{(n-1)T}^{nT}\{\cos[2\pi\theta(t)]+n(t)\}\cos\left(2\pi\hat{f}t\right)dt \\ &\approx AR(\Delta\tau) \\ &\quad\times\int_{(n-1)T}^{nT}\left[\cos\left(2\pi\Delta ft+\pi\mu t^2+2\pi\theta_0\right)+n(t)\right]dt\end{aligned} \tag{5}$$

and

$$\begin{aligned}Q(n) &= \sqrt{2P_r}R(\Delta\tau) \\ &\quad\times\int_{(n-1)T}^{nT}\{\cos[2\pi\theta(t)]+n(t)\}\left[-\sin\left(2\pi\hat{f}t\right)\right]dt \\ &\approx AR(\Delta\tau) \\ &\quad\times\int_{(n-1)T}^{nT}\left[\sin\left(2\pi\Delta ft+\pi\mu t^2+2\pi\theta_0\right)+n(t)\right]dt\end{aligned} \tag{6}$$

where n is the index of the discrete signal samples; A, which stands for the signal amplitude, is equal to $\frac{\sqrt{2P_r}}{2}$; $\hat{f}$ denotes the local frequency replica formed by the receiver numerically controlled oscillator (NCO); $R(\cdot)$ and $\Delta\tau$ denote the auto-correlation function (ACF) of the spreading code and code phase delay error, respectively; Δf represents the Doppler frequency error caused by the difference of frequency between the incoming and local signals, i.e., $\Delta f = f_i + f_d - \hat{f}$. Therefore, the normalized complex form for the signal model after the integration and dump implementation can be given by

$$\begin{aligned}S(n) = &AR(\Delta\tau)\times\frac{1}{T} \\ &\times\int_{(n-1)T}^{nT}\exp\left[j\left(2\pi\Delta ft+\pi\mu t^2+2\pi\theta_0\right)\right]dt \\ &+\tilde{N}(n)\end{aligned} \tag{7}$$

where $\tilde{N}(\cdot)$ stands for the output of the complex Gaussian white noise. Referring to [32], an average angular velocity during the time interval from $(n-1)T$ to nT can be obtained as

$$\bar{\omega}(n) = 2\pi\left(\Delta f+\frac{\mu}{2}nT\right) \tag{8}$$

Accordingly, equation (7) can be approximated as

$$\begin{aligned}S(n) &\approx \frac{1}{T}AR(\Delta\tau)\exp(j2\pi\theta_0) \\ &\quad\times\int_{\left(n-\frac{1}{2}\right)T}^{\left(n+\frac{1}{2}\right)T}\exp[j\bar{\omega}(n)\,t]\,dt+\tilde{N}(n) \\ &= \frac{1}{T}AR(\Delta\tau)\exp(j2\pi\theta_0) \\ &\quad\times\frac{1}{j\bar{\omega}(n)}\exp[j\bar{\omega}(n)\,t]\Big|_{\left(n-\frac{1}{2}\right)T}^{\left(n+\frac{1}{2}\right)T}+\tilde{N}(n) \\ &= \exp\{j\bar{\omega}(n)\,nT+j2\pi\theta_0\} \\ &\quad\times AR(\Delta\tau)\,sinc\left[\bar{\omega}(n)\frac{T}{2}\right]+\tilde{N}(n)\end{aligned} \tag{9}$$

So, the final expression of (7) can be given as follow

$$\begin{aligned}S(n) = &AR(\Delta\tau)\,sinc\left(\Delta fT+\frac{\mu}{2}nT^2\right) \\ &\times\exp\left[j2\pi\left(\theta_0+\Delta fnT+\frac{\mu}{2}n^2T^2\right)\right]+\tilde{N}(n)\end{aligned} \tag{10}$$

Depending on these analysis and associated (10), it could be concluded that the GNSS signal under high dynamics can be assumed as a typical chirp signal model. In this case, the FRFT is introduced to process the signal, and an extra Doppler rate search process will be added besides of the original acquisition cell with respect to the Doppler bin and the code bin.

III. FRFT FOR GNSS SIGNAL

In this section, we firstly introduce the FRFT model and the corresponding FRFT gain for the high-dynamic GNSS signal is derived. Then, a strategy for determining the optimal FRFT order bin is proposed.

A. DEFINITION OF FRFT

The definition of the fractional Fourier transform for signal $x(t)$ is given as follow [14], [37]

$$X(p,u) = \int_{-\infty}^{\infty}x(t)\,K_p(t,u)\,dt \tag{11}$$

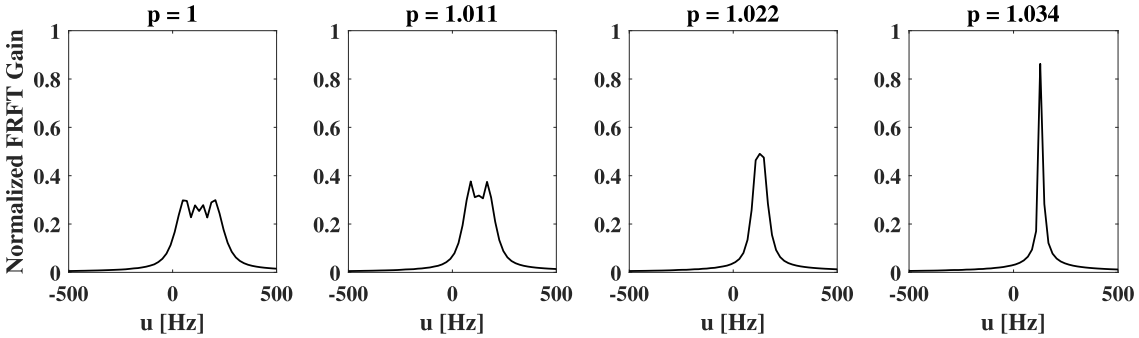

FIGURE 1. DFRFT gain of the high-dynamic GPS L1 C/A signal; τ_d = 51.2 ms, T = 0.2 ms, input real acceleration is −100 g, initial Doppler shift is 0 Hz.

In (11), $K_p(t,u)$ denotes the transformation kernel of FRFT which contains a quadratic term of the independent variable t, and it is defined as

$$K_p(t,u) = \begin{cases} C_\alpha e^{j\pi\left[\left(t^2+u^2\right)\cot\alpha - 2\cdot u\cdot t\cdot\csc\alpha\right]}, & \alpha \neq n\pi \\ \delta(t-u), & \alpha = 2\pi n \\ \delta(t+u), & \alpha = (2n+1)\pi \end{cases} \quad (12)$$

where $C_\alpha = \sqrt{1-j\cot\alpha} = \frac{1}{\sqrt{|\sin\alpha|}}$; p represents the order of FRFT which is an arbitrary real number and $\alpha = \frac{\pi}{2}p$. α can be assumed as a rotation angle from the time-frequency plane in terms of the ordinary Fourier transform (FT) to an extended plane which is formed by the FRFT implementation. When this transformation is done, the power of the LFM signal is expected to converge in the fractional Fourier domain (FRFD), while it will diverge in the ordinary frequency domain. α, or p, in the definition of FRFT corresponds to the estimation process of signal Doppler rate. The discrete fractional Fourier transform of the known GNSS signal (10), $S(n)$, can be defined as [38]

$$X(p,u) = K_p \exp\left(j\pi\cot\alpha u^2\right) \times \sum_{n=0}^{N-1} TS(n)\exp\left(j\pi\cot\alpha(nT)^2 - j2\pi\csc\alpha unT\right) \quad (13)$$

with

$$K_p = C_\alpha \exp\left(j\frac{\alpha}{2} - j\pi\frac{sgn(\sin\alpha)}{4}\right) \quad (14)$$

Equation (10) shows that the high-dynamic GNSS signal can become a typical LFM or chirp signal regardless of the signal dynamic components which are equal to or over the jerk terms. Hence, it is reasonable to introduce the FRFT to process this type of signal, and an extra Doppler rate search process is likely to be added besides of the original acquisition cell with respect to the Doppler bin and the code bin. Accordingly, if the signal is detected by the DFRFT algorithm [15], it can be given by

$$\left\{\hat{p}_x, \hat{u}_x\right\} = \underset{p\in(0,2),u\in\mathbb{R}}{\arg\max}\left|\left\{DF^p[S(n)]\right\}(u)\right| \quad (15)$$

with a certain FRFT order bin, where $\{DF^p[\cdot]\}(u)$ denotes the operator of the digital FRFT proposed by [15]; the associated matched frequency, f_p, can be derived as

$$f_p = \hat{u}_x\csc\hat{\alpha}_x = \hat{u}_x\csc\left(\frac{\pi}{2}\hat{p}_x\right) \quad (16)$$

with

$$\hat{\alpha}_x = \frac{\pi}{2}\hat{p}_x \quad (17)$$

where f_p stands for the detected frequency in FRFD; N denotes the number of samples. Then, the matched Doppler rate obtained by (15), $\hat{\mu}$, can be obtained as

$$\hat{\mu}_x = \zeta\left(\hat{p}_x\right) = -\frac{\cot\left(\hat{\alpha}_x\right)}{NT^2} = -\frac{\cot\left(\hat{\alpha}_x\right)}{\tau_d T} \quad (18)$$

where τ_d is equal to NT, and denotes the search dwell time [39]. τ_d will be frequently used in the following contents. Finally, the Doppler frequency error of signal (10) estimated through (15) and (16), $\Delta\hat{f}$, is given by

$$\Delta\hat{f} = f_p - \frac{1}{2}\hat{\mu}_x NT = f_p - \frac{1}{2}\hat{\mu}_x\tau_d \quad (19)$$

In our work, the digital computation algorithm for FRFT implementation proposed in [15] is adopted here for simulation purpose. A picture to describe how the DFRFT gain of the high-dynamic L1 C/A signal of the global positioning system (GPS) changes with the FRFT order p is illustrated in Fig. 1. When p is equal to 1, the FRFT is equivalent to the ordinary Fourier transform [14], as given in the second property of (65). So, an amplitude peak of the high-dynamic LFM GNSS signal will appear when a proper FRFT order is swept in the FRFD, while it will not occur in an ordinary frequency domain.

B. FRFT GAIN

In this part, the expression with respect to the theoretical FRFT gain for GNSS signal model with linear frequency modulation will be derived.

Substituting (10) to (13) gives the normalized FRFT approximated as

$$|X(p,u)| \approx \underbrace{\left\{\frac{1}{N}\left|\sum_{n=1}^{N} R(\Delta\tau)\right|\right\}}_{R_\Sigma} \times \underbrace{\left\{\frac{1}{TN}\left|\int_0^{NT} sinc(\varphi_t)\,dt\right|\right\}}_{\kappa_1^f} \times \underbrace{\left\{\frac{1}{NT}\left|\int_0^{NT} \exp(j2\pi\delta u t)\,dt\right|\right\}}_{\kappa_2^f} \times \underbrace{\left\{\frac{C_\alpha}{N}\left|\sum_{n=1}^{N} \exp\left[j\pi n^2 T^2(\mu+\cot\alpha)\right]\right|\right\}}_{\kappa_2^\mu} \quad (20)$$

with

$$\varphi_t = \Delta f T + \frac{\mu}{2} T t \quad (21)$$

and the discrete form of δu

$$\delta u = f(u) = \Delta f + \frac{\mu}{2} t - u\csc\alpha \quad (22)$$

where noise term, as mentioned earlier, is zero mean, so, it is removed by average procedure; u stands for frequency spectral parameter of FRFT; δu denotes the error of the frequency or Doppler estimation.

If the auto-correlation attenuation of the code is not neglected, the term of R_Σ for (20) could be deduced by [32]

$$R_\Sigma \approx \begin{cases} 1 - \dfrac{(1+N)\Delta f T}{2 f_r T_c} - \dfrac{\left(2N^2+3N+1\right)\mu T^2}{12 f_r T_c}, \\ \quad \Delta\tau \geq 0 \\ 1 + \dfrac{(1+N)\Delta f T}{2 f_r T_c} + \dfrac{\left(2N^2+3N+1\right)\mu T^2}{12 f_r T_c}, \\ \quad \Delta\tau < 0 \end{cases} \quad (23)$$

where f_r denotes the radio frequency, T_c stands for the code chip interval.

Based on Taylor series expansion and mathematical computations, κ_1^f for (20) satisfies

$$\kappa_1^f = 1 + \frac{{\varphi_0}^2\left({\varphi_0}^2-5\right)}{4} + \frac{\varphi_0\left(2{\varphi_0}^2-5\right)\mu N T^2}{8} + \frac{\left(6{\varphi_0}^2-5\right)\mu^2 N^2 T^4}{48} + \frac{\varphi_0\mu^3 N^3 T^6}{32} + \frac{\mu^4 N^4 T^8}{320} \quad (24)$$

where $\varphi_0 = \Delta f T$.

Again, κ_2^f can be given by

$$\kappa_2^f = sinc(\delta u N T) \quad (25)$$

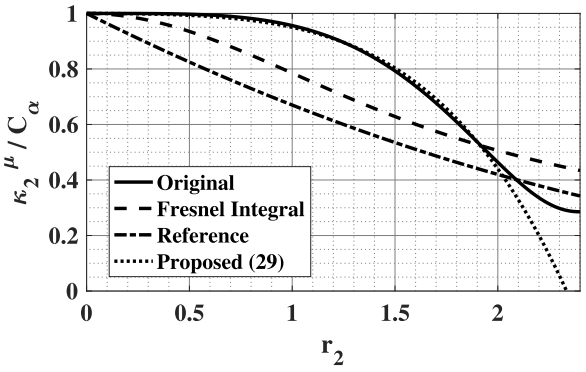

FIGURE 2. Approximated curves with respect to κ_2^μ.

Next, κ_2^μ, which also accounts for (20), can be transferred to the form as [40]

$$\kappa_2^\mu = C_\alpha\left|\frac{1}{r_2}\int_0^{r_2} e^{j\tau^2} d\tau\right| \quad (26)$$

with

$$r_2 = \frac{\sqrt{\pi\cdot\delta\mu}NT}{2} \quad (27)$$

and

$$\delta\mu = \left|\zeta\left(\hat{p}_x\right) - \mu\right| \quad (28)$$

where μ is the real Doppler rate. Using Fresnel integral formula and Taylor series expansion, given

$$\left|\frac{1}{r_2}\int_0^{r_2} e^{j\tau^2} d\tau\right| \approx \left(1 - 0.02{r_2}^2 - 0.03{r_2}^4\right) \quad (29)$$

Therefore, it can be given by

$$\kappa_2^\mu = C_\alpha \cdot \left(1 - 0.02{r_2}^2 - 0.03{r_2}^4\right) \quad (30)$$

as shown in Fig. 2, in which different types of lines correspond to different approximations, i.e., the left side of (29) accounts for Original while Proposed (29) matches with the right side of (29); the expression in terms of Fresnel Integral can be approximated as

$$\left|\frac{1}{r_2}\int_0^{r_2} e^{j\tau^2} d\tau\right| \approx \frac{2\sqrt{\pi}}{3}\frac{erf(r_2)}{r_2} - \frac{1}{3{r_2}^2}\left[1 - \exp\left(-{r_2}^2\right)\right] \quad (31)$$

where $erf(\cdot)$ denotes the error function; then, Reference refers to the approximation extracted from the equation (15) in [40], which is given by

$$\left|\frac{1}{r_2}\int_0^{r_2} e^{j\tau^2} d\tau\right| \approx \left(1 - 0.37 r_2 + 0.04{r_2}^2\right) \quad (32)$$

Equations (23), (24), (25), and (30) can be used to construct an accurate estimator of the Doppler rate. Again, proposed $\frac{\kappa_2^\mu}{C_\alpha}$ obtained from (30), which can almost match with the original expression as given in the left side of (29), (31), or (32), will make a significant difference for the subsequent Doppler rate estimator under high dynamics. More detailed analysis will

be elaborated in subsequent sections. Finally, the proposed normalized theoretical FRFT gain is given by

$$|X(p,u)| \approx R_\Sigma \kappa_1^f \kappa_2^f \kappa_2^\mu \tag{33}$$

More detailed derivations for (33) can be found in Appendix -B.

IV. OPTIMAL FRFT ORDER BIN

The amplitude of digital computation of FRFT process [15] can be perfectly modeled as (33). The long coherent integration is hard to be implemented for the weak GNSS signal under high dynamics. Therefore, fractional Fourier transform technique is proposed to address weak and dynamic GNSS signal acquisition in [32], in which it has been proved that the detection probability can be dramatically improved with the digital FRFT implementation. The digital computational complexity in terms of the Doppler shift search based on the FRFT implementation has also been evaluated in this reference. However, the analysis of the FRFT order bin, which also has a close relationship with the complexity, has been ignored. To solve this problem, we will particularly elaborate on the points of how to determine an optimal FRFT order bin, so that the proposed FRFT acquisition technique could be more feasible to be implemented in a GNSS receiver.

As far as the traditional acquisition algorithm inside the GNSS receiver, two required unknown parameters, i.e., code phase and carrier Doppler, must be roughly estimated. According to the rules of thumb, the Doppler bin size is frequently chosen as $\frac{2}{3\tau_d}$ Hz to guarantee a maximum coherent integration power loss of 3 dB; the code phase bin size is frequently chosen as $\frac{1}{2}$ of the chip duration for GPS L1 C/A signal to guarantee a maximum loss of 3 dB as well [39]. Similarly, an algorithm is proposed to compute the Doppler rate bin size with respect to the FRFT technique, which is known as FRFT order bin or FRFT order search rate in this work. The optimal size of the FRFT order bin can be equivalently contrast to $\frac{2}{3\tau_d}$ for Doppler bin, or $\frac{1}{2}$ for code phase bin as mentioned earlier. The FRFT order bin will be constrained by a certain signal power loss of 6 dB in our proposed algorithm. Once the bin size is determined with this rule, the trade-off between the computational complexity and detection probability in terms of the search dimension for Doppler rate can finally be made. The bin size with the value of 0.001 is frequently used in previous literature [33], [34]. But it is sometimes too small to increase the computation efficiency. The other method, which is called the coarse-to-fine search strategy, is also widely used to decide an optimal FRFT order [35]. However, extra implementations with the digital FRFT should still be added to make decisions on a proper order search rate for this algorithms. In our algorithm, once a priori and coarse Doppler rate range, i.e., $[0g,\ 200g]$, is given, an optimal FRFT order bin can be decided.

In summary, a very small FRFT order bin is commonly decided at first for previous methods, but the reason why such bin size is decided was seldom mentioned. According to [32], the computational complexity will be highly increased by a small FRFT order bin. Since the corresponding optimal code bin and the frequency bin in terms of traditional GNSS acquisition algorithms have access to be decided based on the assumption of a certain signal power loss as explained earlier, the optimal FRFT order bin is also expected to be decided in a similar way. The 6-dB power loss is chosen as the threshold in our work to decide the optimal FRFT order bin and there are two reasons for this choice: firstly, the code phase is assumed to be fully matched with the real value and more tolerance for the power loss is allowed; secondly, such threshold can make full use of the proposed model (29) as given in Fig. 2, and more detailed analysis can be found in the discussions below (38).

When the upper bound of the input Doppler rate is $\bar{\mu}$, the rotation angle, which is related to the maximum FRFT order, $\bar{p}$, can be given by

$$\bar{p} = \zeta^{-1}(\bar{\mu}), \quad \bar{\alpha} = \frac{\pi}{2}\bar{p} \tag{34}$$

subject to

$$\zeta^{-1}(x) \in (0,\ 2) \tag{35}$$

where x denotes the input unknown variable. Referring to (16), the worst resolution for frequency, δu_R, satisfies [15], [38]

$$\delta u_R = \frac{1}{NT\,|\sin\bar{\alpha}|} \tag{36}$$

Again, according to (18), the corresponding Doppler rate resolution, $\delta\mu_R$, could be derived as

$$\delta\mu_R = \left|\bar{\mu} - \zeta\left(\bar{p} + \frac{\Delta p}{2}\right)\right| + \left|\bar{\mu} - \zeta\left(\bar{p} - \frac{\Delta p}{2}\right)\right| \tag{37}$$

where Δp is the FRFT order bin which is assumed as an unknown variable.

The Doppler shift and code phase search processes are included in the regular GNSS signal acquisition implementation. An extra search dimension with respect to the Doppler rate is also contained in our algorithm with the digital FRFT technique. To guarantee a maximum coherent integration power loss of 6 dB based on FRFT algorithm in this work, given

$$10\lg\left[(G_R)^2\right] \geq -6 \Rightarrow G_R \geq 0.5 \tag{38}$$

with

$$G_R = \left|X\left(p, u \middle| p = \zeta^{-1}\left(\frac{\delta\mu_R}{2}\right), u = f^{-1}\left(\frac{\delta u_R}{2}\right)\right)\right| \tag{39}$$

where C_α of κ_2^μ is approximated as $\frac{1}{\sqrt{|\sin\bar{\alpha}|}}$ here.

Since C_α is very close to 1, regardless of the effect of C_α on κ_2^μ, it can be roughly concluded that when $\kappa_2^\mu \geq 0.5$, the proposed model (30) can approximate the original curve as illustrated in Fig. 2. Furthermore, when $\kappa_2^\mu \geq G_R$, the unknown variable, Δp, then, has access to be computed

by (33) and (38). Therefore, the range of the order bin can finally satisfy

$$0 < \Delta p \leq \frac{4}{\pi}\left\{cot^{-1}\left[-2D - \bar{\mu}NT^2\right] - \bar{\alpha}\right\} \tag{40}$$

with

$$\begin{cases} B = \dfrac{2}{3} \\ C = \dfrac{100}{3}\left(\dfrac{\gamma}{R_\Sigma \kappa_1^f \kappa_2^f C_\alpha} - 1\right) \\ \Delta = B^2 - 4C \\ D = -\dfrac{B - \sqrt{\Delta}}{\pi N} \end{cases} \tag{41}$$

subject to

$$\begin{cases} \Delta \geq 0 \\ -B + \sqrt{\Delta} \geq 0 \\ 0 \leq r_2 \leq \sqrt{\dfrac{-B + \sqrt{\Delta}}{2}} \end{cases} \tag{42}$$

where γ is equal to 0.5 as used in (38); r_2 is given by (27). More detailed derivations for (40) can refer to Appendix -C. Given

$$\begin{aligned} \Delta p &= \psi\left(\bar{\mu}, \tau_d, T\right) \\ &= \frac{4}{\pi}\left\{cot^{-1}\left[-2D - \bar{\mu}NT^2\right] - \bar{\alpha}\right\} \end{aligned} \tag{43}$$

where ψ maps $\bar{\mu}$, τ_d, and T to the proposed optimal FRFT order bin.

A report from Jet Propulsion Laboratory (JPL) of National Aeronautics and Space Administration (NASA) in 1988 suggested that the highest dynamic stress determining the upper bound on the performance of some modern agile missiles is an acceleration ramp of 50 g in 0.5 s or jerk for derivative of acceleration of 100 g/s [41]. Therefore, an acceleration threshold ranging from 0 g to 200 g to account for the high-dynamic environment is determined for GNSS signal processing as a priori condition for estimating the optimal FRFT order bin in our work, which is reasonable.

The strategy for determining the optimal FRFT order bin is shown in Algorithm 1 and the associated results are given by Fig. 3, in which different markers correspond to dwell time, τ_d, and colors correspond to sampling interval, T.

After the optimal FRFT order bin is decided, on the condition that the code phase is known, the power peak of the GNSS signal can finally be detected, which satisfies

$$\begin{aligned} \left\{\hat{p}, \hat{u}\right\} &= \underset{p\in(0,2), u\in\mathbb{R}}{\arg\max} \left|\left\{DF^p\left[S\left(n\right)\right]\right\}\left(u\right)\right| \\ \left\{\hat{p}', \hat{u}'\right\} &= \underset{p\in(0,2), u\in\mathbb{R}, p\neq\hat{p}, u\neq\hat{u}}{\arg\max} \left|\left\{DF^p\left[S\left(n\right)\right]\right\}\left(u\right)\right| \end{aligned} \tag{44}$$

with a determined optimal FRFT order bin through Algorithm 1, where $\hat{p}$ and $\hat{u}$ are the quasi-estimations of the real FRFT order and the frequency, respectively; $\hat{p}'$ and $\hat{u}'$ stand for the counterparts of sub-quasi-estimations. Then, substituting $\hat{p}$ to (18) gives the Doppler rate estimation.

Algorithm 1 Strategy for Determining the Optimal FRFT Order Bin

1: **Require**:The maximum estimation error of Doppler frequency with $\{DF^p[\cdot]\}(u)$, $\delta u = \frac{u_R}{2}$; and the maximum estimation error of Doppler rate with $\{DF^p[\cdot]\}(u)$, $\delta\mu = \frac{\mu_R}{2}$;
2: **for** $T = 0.1, 0.2, 0.4\ ms$ **do**
3: **for** $\tau_d = 25.6, 51.2, 102.4, 204.8\ ms$ **do**
4: **for** $\bar{\mu} = 0g, 10hg, 20hg, \cdots 200hg$ **do**
5: Compute the gain R_Σ of (23);
6: Compute the gain κ_1^f of (24);
7: Compute the gain κ_2^f of (25);
8: Compute the gain κ_2^μ of (30);
9: Compute (43) for each case in the loop, i.e., $\Delta p = \psi\left(\bar{\mu}, \tau_d, T\right)$;
10: **end for**
11: **if** $|\psi\left(0, \tau_d, T\right) - \psi\left(200hg, \tau_d, T\right)| > 0.001$ **do**
12: Do not use this case to handle the high-dynamic GNSS signal with acceleration ranging from 0 to 200 g, and remove $\psi\left(\bar{\mu}, \tau_d, T\right)$ to determine a final optimal FRFT order bin;
13: **end if**
14: **end for**
15: **end for**
16: Fix the parameters of τ_d and T, the median value with respect to dynamics is chosen to determine the final optimal FRFT order bin, i.e., $\Delta p_o = \psi\left(100hg, \tau_d, T\right)$.

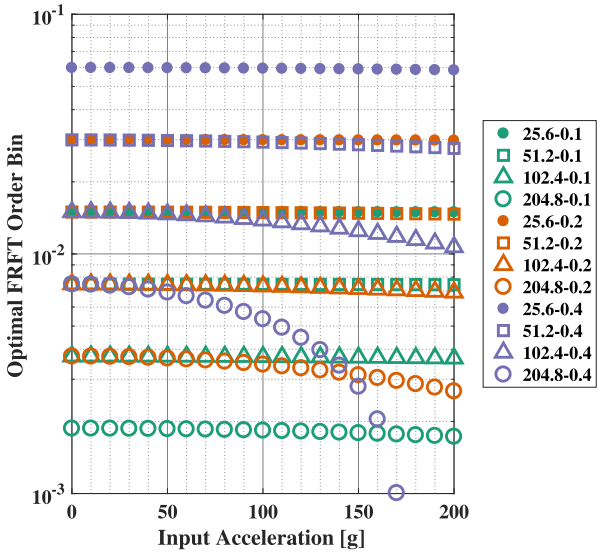

FIGURE 3. Optimal FRFT order bin Δp; numbers correspond to T and τ_d in the legend where they are expressed as τ_d-T.

Whereas, the accuracy of the estimation would typically be reduced by the discrete search processes of $\hat{p}$ and $\hat{u}$.

As illustrated in Fig. 4, where g denotes the gravity, and TC, DS, and SG represent proposed theoretical curves of $|X\left(p, u\right)|$, discrete samples of $|X\left(p, u\right)|$, and corresponding simulated gains, $\left|X\left(\hat{p}, \hat{u}\right)\right|$ [15], respectively, the proposed model $|X\left(p, u\right)|$ is almost consistent with the real gain

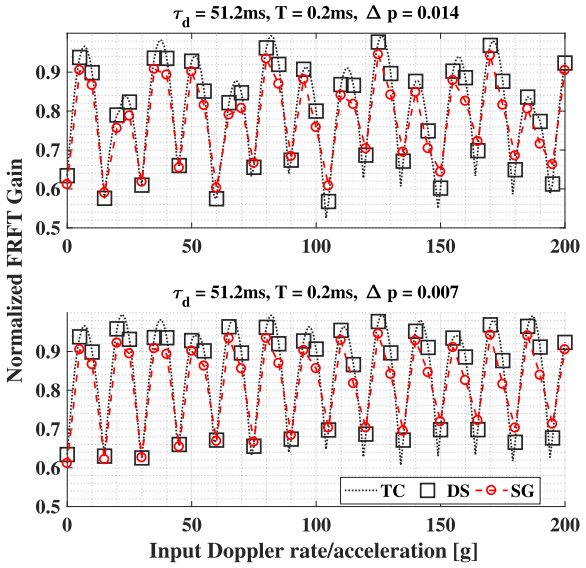

FIGURE 4. Gain comparisons of $|X(p,u)|$ and $|X(\hat{p},\hat{u})|$.

based on the digital FRFT operator, $\{DF^p[\cdot]\}(u)$. So, it can be verified that the proposed model approximates the real value.

As shown in Fig. 5, the red lines describe the FRFT gain trends, when the FRFT order search process is discrete and Doppler shift dimension is assumed to be continuous; the dark lines in the pictures of upper right corner and lower left corner show the trends that what the gain shape will be like, when the frequency resolution increases and simultaneously is gradually close to the real value; the real FRFT gain trend is only consistent with the dark line in the last picture. The curves in Fig. 5 is able to show that both the discrete FRFT frequency dimension and discrete FRFT order dimension make significant contributions to the final digital FRFT implementation results. This fact must be the premise for the subsequent proposed non-linear least square (NLS) algorithm to achieve a Doppler rate estimator. Furthermore, it can also be confirmed that proposed Algorithm 1 is expected to be correct, since the lowest FRFT gain formed with the dark solid at the last sub-picture in Fig. 5 is close to the previously set threshold, i.e., $\gamma = 0.5$. Accordingly, it can be concluded that the final gain is dominated by the FRFT order bin and FRFT frequency bin. Therefore, the theoretical model (33) can almost be used to construct an estimator which provides high-precise Doppler rate estimations.

V. A NOVEL DOPPLER RATE ESTIMATOR

In Section IV, the maximum or optimal FRFT order bin has been calculated as shown in Fig. 3. However, large search intervals with respect to the FRFT order will finally reduce the estimation accuracy of the Doppler rate by using digital FRFT operator with (44). Based on previous analysis locating at last of Section IV, an approach can be proposed to significantly improve the Doppler rate accuracy in this situation.

A. SYSTEM MODEL FOR NLS ESTIMATION

Firstly, a loss function is given by

$$\begin{aligned} &J(\theta) \\ &= \left| \left| X\left(p, u | p = \zeta^{-1}(\mu), u = f^{-1}(\delta u)\right) \right| - \tilde{P} \right|^2 \\ &= \left| R_\Sigma \kappa_1^f C_\alpha sinc(\delta u N T) \left(1 - 0.02 s_{\delta\mu} - 0.03 s_{\delta\mu}^2\right) - \tilde{P} \right|^2 \end{aligned} \tag{45}$$

with

$$\begin{cases} s_{\delta\mu} = \dfrac{\pi}{4} \delta\mu N^2 T^2 \\ \theta = [\delta u,\ \delta\mu]^T \end{cases} \tag{46}$$

where δu of (22) and $\delta\mu$ of (28) are unknown variables for Doppler shift error and Doppler rate error in FRFD, respectively; $\tilde{P}$ is the detected amplitude of the incoming signal by the digital FRFT implementation with (44).

We can notice that the original loss function is a non-linear case which is hard to be handled. So, the Taylor series expansion is used to yield a linearized form, which can be approximated as

$$\begin{aligned} J(\theta, \xi) \approx J(\theta_0, \xi) &+ \left.\frac{\partial J(\theta, \xi)}{\partial \delta u}\right|_{\theta=\theta_0} (\delta u - \delta u_0) \\ &+ \left.\frac{\partial J(\theta, \xi)}{\partial \delta\mu}\right|_{\theta=\theta_0} (\delta\mu - \delta\mu_0) \end{aligned} \tag{47}$$

where ξ is the input vector obtained from (44), which is $\xi = [p, u]^T$; the subscripts of 0 denote the initial value of the unknown states; the design matrix is finally given by

$$G = \begin{bmatrix} \left.\dfrac{\partial J(\theta, \xi^{(1)})}{\partial \delta u}\right|_{\theta=\theta_0} & \left.\dfrac{\partial J(\theta, \xi^{(1)})}{\partial \delta\mu}\right|_{\theta=\theta_0} \\ \vdots & \vdots \\ \left.\dfrac{\partial J(\theta, \xi^{(i)})}{\partial \delta u}\right|_{\theta=\theta_0} & \left.\dfrac{\partial J(\theta, \xi^{(i)})}{\partial \delta\mu}\right|_{\theta=\theta_0} \end{bmatrix}_{i\times 2} \tag{48}$$

where i represents the order of the input vector. Detailed derivations for (47) is offered in Appendix -D.

Next, the state vector, Δx, can be given by

$$\Delta x = [\Delta\delta u,\ \Delta\delta\mu]^T = [\delta u - \delta u_0,\ \delta\mu - \delta\mu_0]^T \tag{49}$$

and the measurement misclosure vector, b, satisfies

$$b = [J\left(\theta, \xi^{(1)}\right), \cdots, J\left(\theta, \xi^{(i)}\right)]^T \tag{50}$$

In this research, only two measurements are contained; relying on (44), they are given by

$$\begin{cases} \tilde{P}_m = \left|X\left(\hat{p}, \hat{u}\right)\right| \\ \tilde{P}'_m = \left|X\left(\hat{p}', \hat{u}'\right)\right| \end{cases} \tag{51}$$

In this case, $i = 2$. These two measurements are included in b referring to (45). Accordingly, the solutions can be obtained using non-linear least square method as follow [42]

$$\Delta\hat{x} = \left(G^T G\right)^{-1} G^T b \tag{52}$$

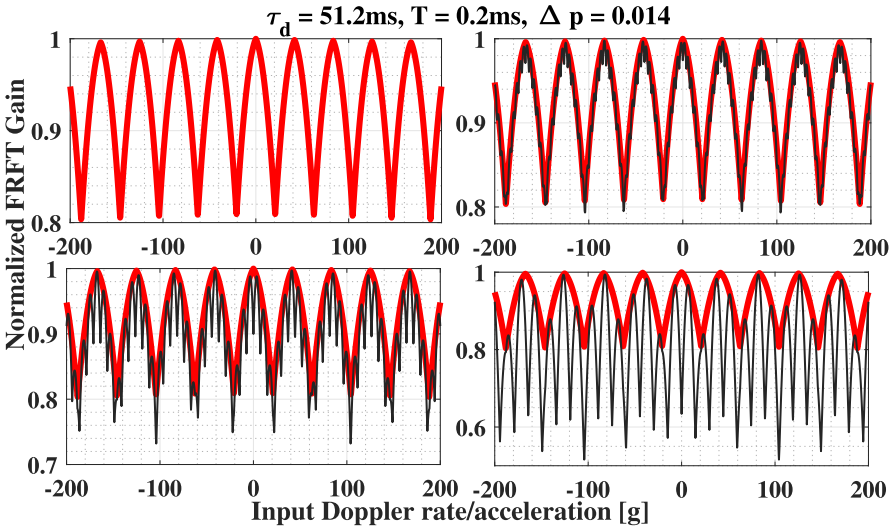

FIGURE 5. Gain transition trends w.r.t. frequency resolution with a fixed optimal FRFT order bin.

B. IMPLEMENTATION OF PROPOSED DOPPLER RATE ESTIMATOR

The proposed Doppler rate estimator based on FRFT with NLS method is summarized in Algorithm 2. It should be noticed that half of the optimal FRFT order bin computed through Algorithm 1, i.e., $\frac{\Delta p_o}{2}$, is expected to be determined as the final order search bin in the digital FRFT implementation for our proposed Doppler rate estimator, as provided by Step 4 in Algorithm 2. In order to elaborate the reason why the strategy is adopted, an extreme case with respect to the digital FRFT implementation for Algorithm 2 is shown in Fig. 6.

On the one hand, two unknown variables are contained in the state vector, (49), of the NLS model. Therefore, minimum two measurements should be involved in the estimation process to require a full rank of the NLS solution.

On the other hand, as mentioned in Section V-A, $\tilde{P}_m$ and $\tilde{P}'_m$ are two measurements of the NLS estimation. Only when $\left|X\left(\hat{p},\hat{u}\right)\right| > 0.5$ and $\left|X\left(\hat{p}',\hat{u}'\right)\right| > 0.5$, can the proposed $|X\ (p,\ u)|$ be used to approximate them, as explained below (38).

Based on these analysis, if a full optimal FRFT order bin, which is obtained through Algorithm 1, is chosen as the order search bin during the digital FRFT implementation, the case when both $\tilde{P}_m$ and $\tilde{P}'_m$ are larger than 0.5 will be very hard to occur as shown in Fig. 6. Therefore, half of the optimal FRFT order bin, $\Delta p = \frac{\Delta p_o}{2}$, should be used in Algorithm 2 to confirm that the estimation result is reliable enough.

As mentioned earlier, the absolute value of Doppler rate for the high-dynamic GNSS signal can be assumed to range from 0 to 200g in this work, so, the search range of the FRFT order is subject to

$$p \in \left[\zeta^{-1}\left(200hg\right),\ \zeta^{-1}\left(-200hg\right)\right] \tag{53}$$

The outliers sometimes occur after the NLS process, so, the blunder check algorithm needs to be contained in the implementation. As mentioned earlier, the FRFT order search

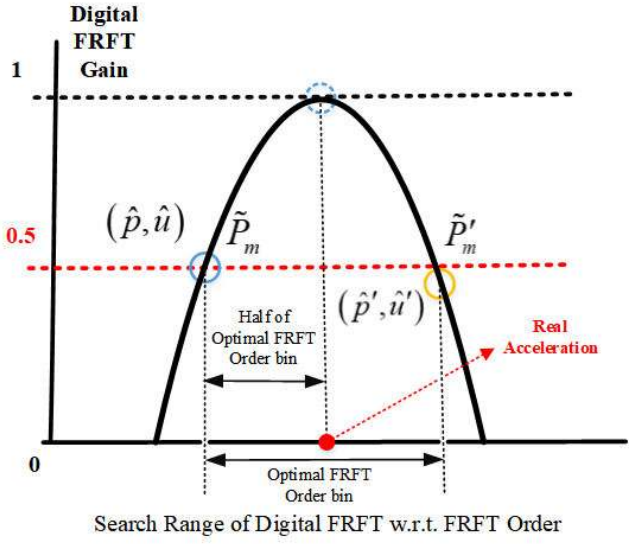

FIGURE 6. An extreme case w.r.t. the digital FRFT implementation for Algorithm 2.

bin is half of the value with the computed optimal order bin, i.e., $\frac{\Delta p_o}{2}$. Based on the previous analysis and simulation results as shown in Fig. 2 and Fig. 4, the proposed NLS method can be assumed to be unbiased. Again, according to the central limit theorem [43], the standard deviation (STD) of the Doppler rate estimation error, σ_μ, should be mainly caused by half of the FRFT order bin size. Besides, since $\frac{\Delta p}{4}$ is expected to be small enough, σ_μ can finally be approximated as

$$\begin{aligned}\sigma_\mu &\approx \left|\zeta\ (p) - \zeta\left(p + \frac{\Delta p}{4}\right)\right| \\ &\approx \left|\zeta\ (p) - \zeta\left(p - \frac{\Delta p}{4}\right)\right| \\ &\approx \frac{\left|\zeta\ (p) - \zeta\left(p + \frac{\Delta p}{4}\right)\right| + \left|\zeta\ (p) - \zeta\left(p - \frac{\Delta p}{4}\right)\right|}{2}\end{aligned} \tag{54}$$

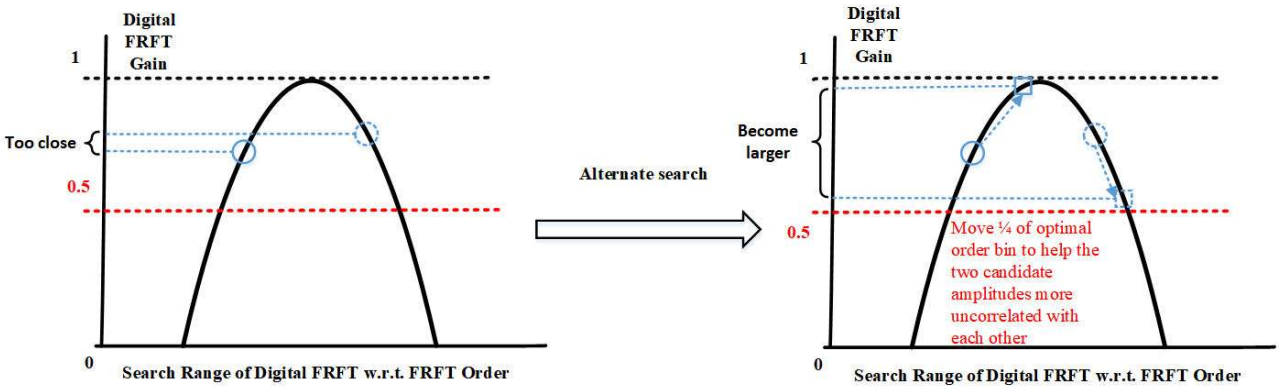

FIGURE 7. First case for alternate search procedure with digital FRFT implementation.

where p corresponds to the real Doppler rate or acceleration. Similarly, the STD of f_p can be approximated as

$$\sigma_u = \frac{1}{4NT\left|\sin\left(\frac{\pi}{2}p\right)\right|} \tag{55}$$

Referring to (54), (55) and (19), the variance of the Doppler shift estimation, $\Delta\hat{f}$, for the original digital FRFT implementation can be derived as follow

$$\begin{aligned}\sigma_{\Delta f}^2 &= var\left(\Delta\hat{f}\right)\\ &= var\left(f_p\right) + \frac{N^2T^2}{4}\cdot var\left(\hat{\mu}\right)\\ &\approx \sigma_u^2 + \frac{N^2T^2}{4}\cdot\sigma_\mu^2\end{aligned} \tag{56}$$

Finally, the STD of $\Delta\hat{f}$ can be obtained as

$$\sigma_{\Delta f} = \sqrt{\sigma_u^2 + \frac{N^2T^2}{4}\cdot\sigma_\mu^2} \tag{57}$$

In this research, 3σ rule will be used to make decisions. If the NLS result manages to pass the blunder check procedure, based on (18) and (44), the Doppler rate estimation can be finally given as follow

$$\hat{\mu} = \zeta\left(\hat{p}\right) + \Delta\delta\hat{\mu} \tag{58}$$

where $\Delta\delta\hat{\mu}$ is estimated by (52). Then, based on (16), (19), and (44), the initial Doppler shift estimation can be given by

$$\Delta\hat{f} = \hat{u}\csc\left(\frac{\pi}{2}\hat{p}\right) - \frac{1}{2}\hat{\mu}NT + \Delta\delta\hat{u} \tag{59}$$

where $\Delta\delta\hat{u}$ is also estimated by (52).

C. ALTERNATE SEARCH PROCEDURE

In Algorithm 2, the values of $\left[\tilde{P}_m,\ \tilde{P}'_m\right]$ are possible to be very close to each other, and this fact can lead to the consequence of singular estimation results. An alternate search procedure, as illustrated in Fig. 7, is introduced to alleviate the given problem. In this figure, two blue circles correspond to two samples of $\left[\tilde{P}_m,\ \tilde{P}'_m\right]$ before the alternate search procedure, while two blue squares represent the counterparts of the samples when the alternate search procedure is done. On the other hand, if the amplitude difference between two candidate samples is firstly large enough, this property would not be influenced by the alternate search procedure so much as shown in Fig. 8.

Algorithm 2 A Novel Doppler Rate Estimator

1: **Require**: Determined optimal FRFT order bin Δp through Algorithm 1; the normalized acquisition process.
2: Initialize p with lower bound of FRFT order search range;
3: **while** p satisfies (53) **do**
4: $\quad p = p + \frac{\Delta p_o}{2}$
5: $\quad$ Implement the digital computation of FRFT;
6: **end while**
7: Implement (44) with results from steps 2 to 6;
8: Obtain signal amplitudes with (51);
9: Compute the design matrix, G, by (48);
10: Build the measurement misclosure vector, b, by (50);
11: Estimate the frequency error, $\Delta\delta\hat{u}$, and Doppler rate error, $\Delta\delta\hat{\mu}$, of the unknown state vector, $\Delta\hat{x}$, based on NLS method by (52);
12: Compute σ_μ by (54) for blunder check;
13: **if** $\left|\Delta\delta\hat{\mu}\right| \le 3\sigma_\mu$ **do**
14: $\quad$ Compute the accurate Doppler rate by (58);
15: $\quad$ Compute the initial Doppler shift by (59);
16: **else do**
17: $\quad \hat{\mu} = \zeta\left(\hat{p}\right)$, by (18);
18: $\quad$ Compute the initial Doppler shift by (19).
19: **end if**

Therefore, an alternate search procedure is added after Algorithm 2 to efficiently reduce the probability of singular NLS estimations. The expressions for alternate search procedure can be given by

$$\begin{cases}\left\{DF^{\hat{p}+\frac{\Delta p_o}{4}}\left[S\left(n\right)\right]\right\}\left(\hat{u}\right)\\ \left\{DF^{\hat{p}-\frac{\Delta p_o}{4}}\left[S\left(n\right)\right]\right\}\left(\hat{u}\right)\end{cases} \tag{60}$$

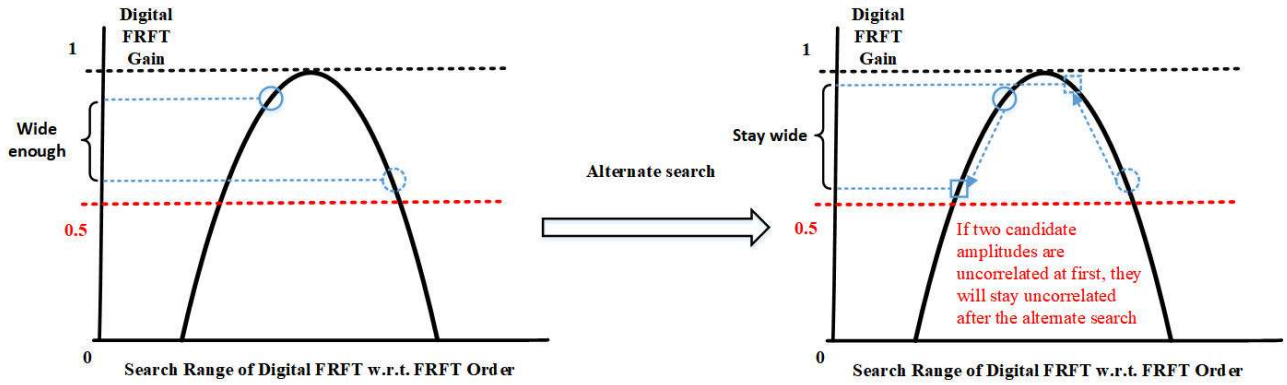

FIGURE 8. Second case for alternate search procedure with digital FRFT implementation.

Accordingly, given

$$\hat{p}_{alt} = \arg\max \left\{ \begin{array}{l} \left| \left\{ DF^{\hat{p}+\frac{\Delta p_o}{4}} [S(n)] \right\} (\hat{u}) \right|, \\ \left| \left\{ DF^{\hat{p}-\frac{\Delta p_o}{4}} [S(n)] \right\} (\hat{u}) \right| \end{array} \right\} \tag{61}$$

Then, the associated alternate FRFT gains are given as follow

$$\begin{cases} \tilde{P}_{alt} = \max \left[\left| X\left(\hat{p} + \dfrac{\Delta p_o}{4}, \hat{u}\right) \right|, \left| X\left(\hat{p} - \dfrac{\Delta p_o}{4}, \hat{u}\right) \right| \right] \\ \tilde{P}'_{alt} = \min \left[\left| X\left(\hat{p} + \dfrac{\Delta p_o}{4}, \hat{u}\right) \right|, \left| X\left(\hat{p} - \dfrac{\Delta p_o}{4}, \hat{u}\right) \right| \right] \end{cases} \tag{62}$$

So, the Doppler rate estimation based on the measurements of (62) is given by

$$\hat{\mu}_{alt} = \zeta\left(\hat{p}_{alt}\right) + \Delta\delta\hat{\mu}_{alt} \tag{63}$$

and the corresponding Doppler shift estimation is given by

$$\Delta\hat{f}_{alt} = \hat{u}\csc\left(\frac{\pi}{2}\hat{p}_{alt}\right) - \frac{1}{2}\hat{\mu}_{alt}NT + \Delta\delta\hat{u}_{alt} \tag{64}$$

where $\Delta\delta\hat{u}_{alt}$ and $\Delta\delta\hat{\mu}_{alt}$ represent estimations of Doppler shift error and Doppler rate error related to (62), respectively.

Finally, the criterion for the alternate search procedure is summarized in Algorithm 3.

Algorithm 3 Alternate Search Procedure

Require: $\Delta\delta\hat{u}$, $\Delta\delta\hat{\mu}$ and σ_μ through Algorithm 2;
Implement alternate digital FRFT algorithm with (60);
Obtain $\left[\tilde{P}_{alt},\ \tilde{P}'_{alt}\right]$ by (62);
Compute the design matrix, G, by (48);
Build the measurement misclosure vector, b, by (50);
Estimate the frequency error, $\Delta\delta\hat{u}_{alt}$, and Doppler rate error, $\Delta\delta\hat{\mu}_{alt}$, of the unknown state vector based on NLS method by (52);
if $\left|\Delta\delta\hat{\mu}\right| < \left|\Delta\delta\hat{\mu}_{alt}\right|$ **do**
  if $\left|\Delta\delta\hat{\mu}\right| < 3\sigma_\mu$ **do**
    Compute the accurate Doppler rate by (58);
    Compute the initial Doppler shift by (59);
  else do
    Compute the Doppler rate by (18);
    Compute the initial Doppler shift by (19).
  end if
else do
  if $\left|\Delta\delta\hat{\mu}_{alt}\right| < 3\sigma_\mu$ **do**
    Compute the accurate Doppler rate by (63);
    Compute the initial Doppler shift by (64);
  else do
    Compute the Doppler rate by (18);
    Compute the initial Doppler shift by (19).
  end if
end if

VI. INTRODUCTION OF THE PROPOSED ALGORITHMS

We introduce three algorithms in this section, and we explain them through a flow chart as illustrated in Fig. 9, where the red lines highlight the main flow for the estimation process of the unknown initial Doppler shift and Doppler rate of the incoming GNSS signal. Required input information are also shown in the other blocks of this chart. A summary for this flow chart will be subsequently provided. At first, Algorithm 1 is used to calculate the proposed optimal bin size of the FRFT order with the priori information about the range of the signal dynamics. The computed bin size can guarantee a maximum 6-dB loss of the DFRFT in the acquisition process as mentioned earlier in Section IV. Then, Algorithm 2 proposes a novel and fast Doppler rate estimator with the NLS method based on the DFRFT implementation. At last, the alternate estimations of the Doppler shift and Doppler rate unknown variables would be attained with Algorithm 3 as well. The decision making process will be done and the proper estimations would be simultaneously determined with Algorithm 3.

VII. SIMULATION RESULTS

GPS L1 C/A signal is adopted to verify proposed algorithms, and Matlab R2016b is the software platform used for simulations. Only carrier and spreading code are included

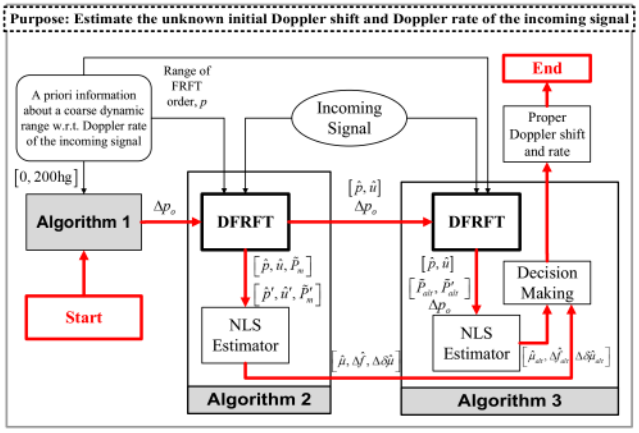

FIGURE 9. An overall flow chart for the proposed three algorithms, i.e., Algorithm 1, Algorithm 2, and Algorithm 3.

TABLE 1. Parameter settings for simulations.

Software Platform	Matlab R2016b
GNSS Signal Type	GPS L1 C/A
Intermediate Frequency	11.605 MHz
Sampling Rate	15.5 MHz
Radio Frequency	1575.42 MHz
Code Rate	1.023 MHz
Input Initial Code Phase	50 Chips
Input Initial Doppler Shift	0 Hz
Input Acceleration (Absolute Value)	0 g to 200 g
Gravity (g)	9.80665 m/s^2
Speed of Light	299792458.0 m/s
Input C/N_0 (Fig. 11)	28 dB-Hz to 43 dB-Hz
Input C/N_0 (Fig. 10 to Fig. 14)	43 dB-Hz

in simulated signals. In reality, assisted GNSS (A-GNSS) technology, by which navigation data can be retrieved from an Internet server through Wifi/cellular network [44], is frequently used to obtain the data-wipe-off signal for a very long coherent integration in a challenging environment [45]–[47]. Besides, some other techniques are also able to address the data-bit-transition problem, e.g., the proposed approach in [3]. Therefore, it is reasonable that data bits are ignored in our simulations. The false alarm rate is set to 10^{-6}. Input initial Doppler shift is 0 Hz. Experiments will be only carried out when the signal is detected. Since the acquisition process in terms of the spreading code dimension is not related to this work, it is assumed that the code phase is acquired in simulations. The parameter settings are listed in Table 1.

Referring to Algorithm 1 and the associated results illustrated in Fig. 3, four cases are chosen to verify the proposed algorithms, i.e., Algorithms 2 and 3. The associated parameter settings are listed in Table 2 where the upper and lower bounds of p with the given acceleration ranges are primarily estimated and constrained by the computation results of (53). It should be noticed that just the cases with positive accelerations are included in simulations. Explanations for this choice will be subsequently described.

Suppose that the operator for continuous FRFT is given by $R^{\alpha}(\cdot)$; $F(\cdot)$ is the operator for the ordinary Fourier transform. As mentioned in [14], $R^{\alpha}(\cdot)$ and $F(\cdot)$ should have the following properties

$$\begin{cases} F\{F[x(t)]\} = x(-t) \\ R^{\frac{\pi}{2}}[x(t)] = F[x(t)] \\ R^{\beta}\{R^{\alpha}[x(t)]\} = R^{\alpha+\beta}[x(t)] \\ X(p,-u) = R^{\frac{\pi}{2}p}[x(-t)] \end{cases} \tag{65}$$

where $x(t)$ stands for a signal in the time domain. According to these properties, it can be derived as

$$\begin{aligned} X(p+2,u) &= R^{\alpha+\pi}[x(t)] \\ &= R^{\alpha}\left\{R^{\pi}[x(t)]\right\} = R^{\alpha}\{F\{F[x(t)]\}\} \\ &= R^{\alpha}[x(-t)] = X(p,-u) \end{aligned} \tag{66}$$

where $\alpha = \frac{\pi}{2}p$; $X(p,u)$ denotes the FRFT output of $x(t)$ with a rotation angle of α, or with a FRFT order of p. $|X(p,u)|$ is periodic with period π in terms of the rotation angle. Accordingly, it is appropriate that the DFRFT is carried out within a single period in terms of the sweeping search interval, i.e., $\alpha \in [0,\pi]$. Furthermore, depending on (18) and the property of cotangent, it can also be obtained as

$$\mu = \begin{cases} \zeta(p) \geq 0, & p \in [1,2) \\ \zeta(p) \leq 0, & p \in (0,1] \end{cases} \tag{67}$$

where μ denotes the Doppler rate of the signal. Again, according to the property of the cotangent function, it can be derived as

$$\zeta(p) = -\zeta(2-p) \tag{68}$$

Then, if $\zeta(p) \leq 0$ with $p \in (0,1]$, substituting (68) to it gives $\zeta(2-p) \geq 0$ with $2-p \in [1,2)$, i.e., $\zeta(p') \geq 0$ with $p' \in [1,2)$ and $p' = 2-p$. The derivation result means that the estimated positive Doppler rate has access to be equivalent to the negative one, vice versa, i.e., $\left|X\left(2-\zeta^{-1}(-\mu),u\right)\right| = \left|X\left(\zeta^{-1}(\mu),u\right)\right|$. Therefore, the FRFT amplitude of $|X(p,u)|$ with positive dynamics are symmetric with the one with negative dynamics, which means that they are dual with the zero-acceleration solution, where the case with detected $p = 1$ corresponds to the one that the acceleration is equal to zero. So, it is reasonable that the simulations in which only the single period with respect to the sign of the Doppler rate are implemented. Fig. 5 can help to understand this story.

A. ROOT-MEAN-SQUARE ERROR FOR ESTIMATIONS

Some simulation results are illustrated in Fig. 10 and Fig. 11, where opt-frft denotes the original DFRFT operator, i.e., $\{DF^{p}[S(n)]\}(u)$, with the determined optimal FRFT order bin given as $\Delta p = \frac{\Delta p_o}{2}$; opt-frft-nls stands for the result computed with Algorithms 2 which is based on the

TABLE 2. Simulation parameter settings for digital FRFT implementation.

Simulation cases	Range of p	T [ms]	τ_d [ms]	Optimal order bin	Order search bin
Case 1	0.986 to 1.028	0.1	25.6	0.0149	0.007
Case 2	0.972 to 1.056	0.2	25.6	0.0293	0.014
Case 3	0.972 to 1.168	0.4	51.2	0.0293	0.014
Case 4	0.986 to 1.084	0.2	51.2	0.0149	0.007

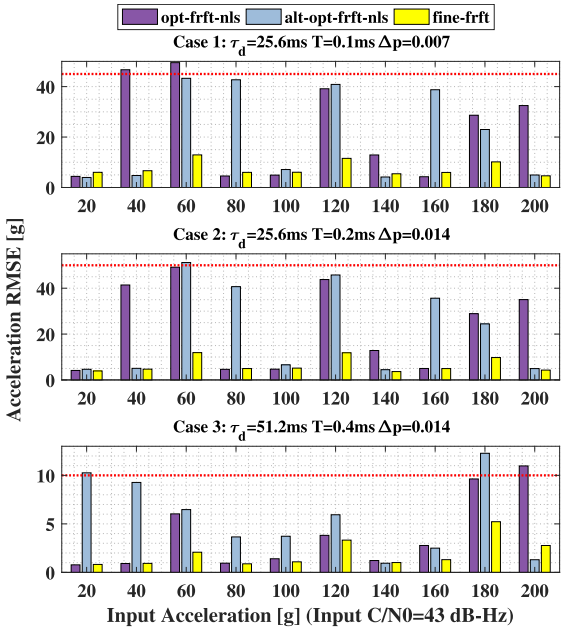

FIGURE 10. Monte Carlo simulation performances for Case 1, 2, and 3. Displayed accelerations for the x-axis are the absolute values of the real input accelerations.

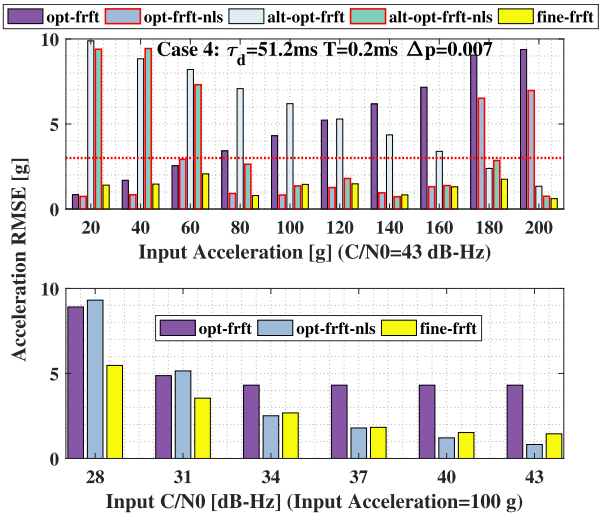

FIGURE 11. Monte Carlo simulation performances for Case 4. Displayed accelerations for the x-axis are the absolute values of the real input accelerations.

NLS estimation; alt-opt-frft represents the alternate counterparts with $\left\{DF^{\hat{P}_{alt}}\left[S\left(n\right)\right]\right\}\left(\hat{u}\right)$ of opt-frft; alt-opt-frft-nls denotes the result corresponded to the alternate search of opt-frft-nls, of which the computation process is given in Algorithm 3; fine-frft is the original operator $\{DF^{p}\left[S\left(n\right)\right]\}\left(u\right)$ with a fine FRFT order bin size, i.e., the value of 0.001. The dashed red lines in Fig. 10 and Fig. 11 highlight the proposed maximum root-mean-square error (RMSE) among the cases with different input accelerations. 100 trials are contained for each experiment in Fig. 10 and Fig. 11.

Through the Monte Carlo experiment results in Fig. 10 and Fig. 11, it can be roughly concluded that the results with proposed algorithms for Case 1 and Case 2 perform worse than the ones with fine-frft; the results for Case 3 are similar to the ones for Case 4 considering the average RMSE results. However, the maximum RMSE of Case 3 is larger than the error of Case 4. It can be accordingly inferred that the proposed algorithms are more efficient in Case 4 than in Case 3. In this case, Case 4 is finally determined to test how the performance of proposed algorithms change with different input C/N_0 values. As illustrated in the bottom of Fig. 11, the lower the C/N_0 is, the worse the proposed algorithms perform. It should be noticed that the performance of the acquisition based on the digital FRFT implementation for the weaker-signal situation can be improved by increasing the dwell search time [32].

When the real input acceleration is fixed, the theoretical lower bound (LB) for Doppler rate and Doppler shift estimation based on the digital FRFT implementation is approximated as (54) and (57), respectively. Based on the analysis of the stochastic model [48], the mean of STD for Doppler rate estimation among the full acceleration search dimension can be derived as follow

$$\bar{\sigma}_{\mu}=\sqrt{\frac{\sum_{i=1}^{M}\left(\sigma_{\mu}^{(m)}\right)^{2}}{M}} \tag{69}$$

where the superscript m corresponds to the index of the input acceleration; M stands for the number of input acceleration. Similarly, the mean of STD for Doppler shift estimation can be given by

$$\bar{\sigma}_{\Delta f}=\sqrt{\frac{\sum_{i=1}^{M}\left(\sigma_{\Delta f}^{(m)}\right)^{2}}{M}} \tag{70}$$

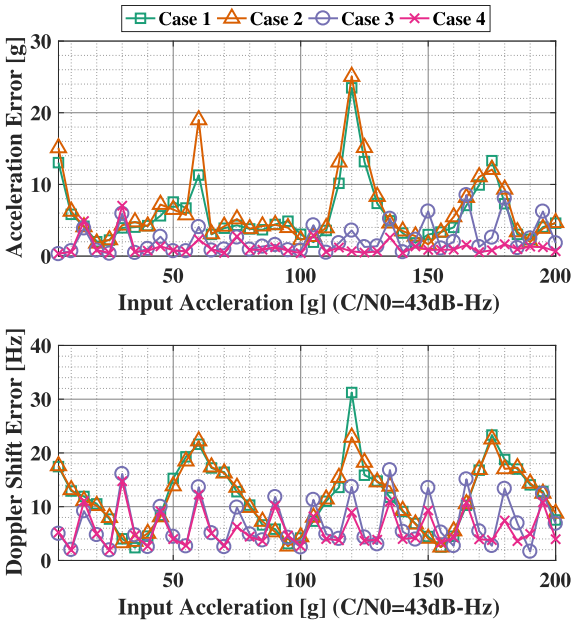

FIGURE 12. RMSE for Doppler rate and Doppler shift estimations based on Monte Carlo experiments with proposed algorithms. Displayed accelerations for the x-axis are the absolute values of the real input accelerations.

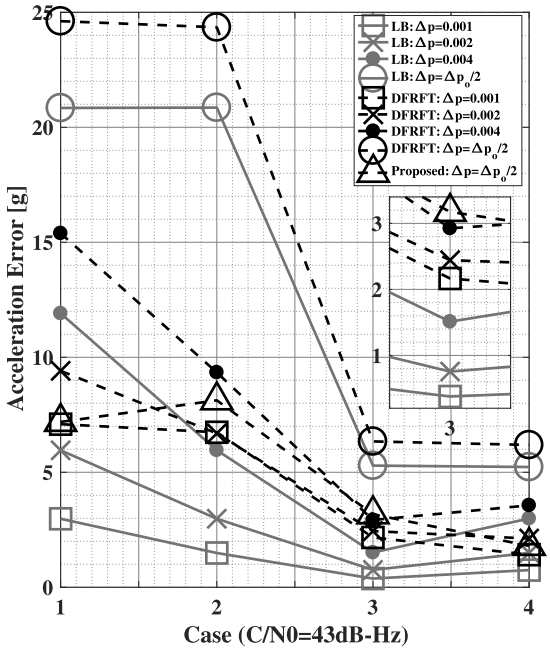

FIGURE 13. Mean of RMSE for Doppler Rate estimations based on Monte Carlo experiments.

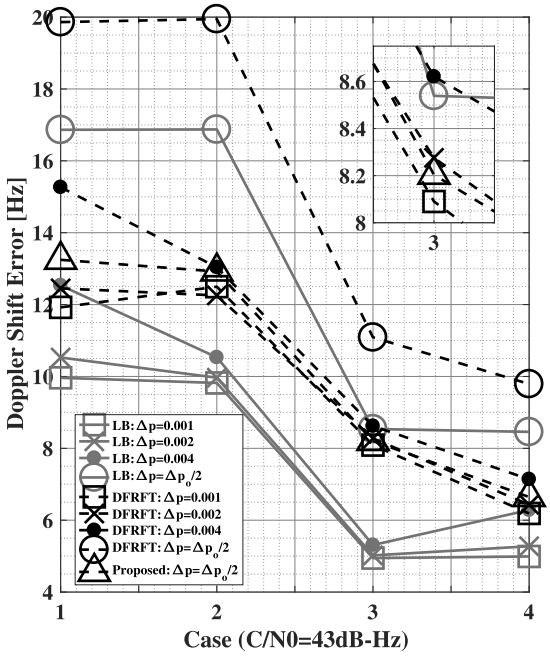

FIGURE 14. Mean of RMSE for Doppler shift estimations based on Monte Carlo experiments.

Another group of Monte Carlo experiments are carried out to verify the estimation accuracy with proposed algorithms. Firstly, the RMSE curves estimated from the experiment results with proposed algorithms as given in Fig. 9 are illustrated in Fig. 12. It can be found that the RMSEs for Case 1 and Case 2 perform similarly with each other; the estimation performances are also addressed similarly within Case 3 and Case 4. Besides, it is assured that the results of Case 3 and Case 4 outperform the ones computed from Case 1 and Case 2 as shown in Fig. 12.

In addition, considering that the input dynamics ranging from 0 g to 200 g, the means of the RMSE for all these estimations are computed with (69) and (70), and the results of Doppler rate estimation errors and initial Doppler shift estimation errors are shown in Fig. 13 and Fig. 14, respectively, where LB denotes the theoretical lower bound computed with (69) and (70). At first, the estimation trends of the simulation data are almost matched with the curves of the theoretical lower bound. Besides, there is a noticeable error difference between the LB and the practical mean of the RMSE, because the noise level is omitted here. However, the random noise should also be assumed as a factor that would contribute to the value of the LB in this work.

B. COMPUTATIONAL COMPLEXITY

To verify the improvement of the computation efficiency with proposed algorithms, the computational complexity with different methods will be analyzed in this section.

The computational complexities for proposed Algorithm 2 and Algorithm 3 will be analyzed. The most time-consuming step for computation is supposed to be the procedure of the NLS estimation with (52), which contains twice matrix multiplication and once matrix inversion, regardless of the process with the digital FRFT implementation. As mentioned in [49], the computational complexity for both matrix multiplication and inversion implementations should be given by $\Theta\left(i^3\right)$, where $\Theta(\cdot)$ is the notation for time complexity; i stands for the matrix dimension which is equal to 2 in proposed algorithms. Again, seven-times iterations are used to confirm a reliable convergence for the NLS estimation

process. Therefore, the computational complexity with (52) can be obtained as follow

$$O_{nls} = 7 \times 3 \times \Theta\left(2^3\right) = 21 \cdot \Theta\left(2^3\right) \tag{71}$$

Next, referring to [32], the computational complexity for the digital FRFT algorithm is given by

$$O = \frac{p_r}{2\Delta p}\left[\frac{18\tau_d}{T}\log_2\left(\frac{\tau_d}{T}\right) + \frac{34\tau_d}{T}\right] \tag{72}$$

where p_r denotes the search range of FRFT order.

The computation process for proposed algorithms in Case 4 will be subsequently taken to be an example. Firstly, the corresponding complexity with respect to Algorithm 2 can be obtained as

$$\begin{aligned} O_1 &= \frac{p_r}{2 \times \frac{\Delta p_o}{2}}\left[\frac{18\tau_d}{T}\log_2\left(\frac{\tau_d}{T}\right) + \frac{34\tau_d}{T}\right] \\ &= \frac{1.084 - 0.986}{2 \times 0.007} \\ &\quad \times \left[\frac{18 \times 51.2}{0.2} \times \log_2\left(\frac{51.2}{0.2}\right) + \frac{34 \times 51.2}{0.2}\right] \\ &= 318976 \end{aligned} \tag{73}$$

Then, the time complexity in terms of the NLS estimation has been offered with (71). Finally, extra added computational complexities in Algorithm 3 compared with Algorithm 2 will be given by

$$\begin{aligned} O_2 &= 2\left[\frac{18\tau_d}{T}\log_2\left(\frac{\tau_d}{T}\right) + \frac{34\tau_d}{T}\right] \\ &= 2 \times \left[\frac{18 \times 51.2}{0.2} \times \log_2\left(\frac{51.2}{0.2}\right) + \frac{34 \times 51.2}{0.2}\right] \\ &= 91136 \end{aligned} \tag{74}$$

Therefore, the final computational complexity for proposed algorithms, i.e., Algorithm 2 plus Algorithm 3, can be summarized as

$$O_p = O_1 + O_{nls} + O_2 = 410112 + 21 \cdot \Theta\left(2^3\right) \tag{75}$$

As shown in Fig. 13 and as listed in Table 3, the estimation accuracy with proposed algorithms in Case 4 performs better than the original FRFT implementation with an order search rate of 0.002 but worse than the one with an order search rate of 0.001. The computational complexities for these two FRFT implementation processes are given by

$$\begin{aligned} O_0 &= \frac{p_r}{2\Delta p}\left[\frac{18\tau_d}{T}\log_2\left(\frac{\tau_d}{T}\right) + \frac{34\tau_d}{T}\right] \\ &= \frac{0.098}{2 \times 0.001} \times \left[\frac{18 \times 51.2}{0.2} \times \log_2\left(\frac{51.2}{0.2}\right) + \frac{34 \times 51.2}{0.2}\right] \\ &= 2232832 \end{aligned} \tag{76}$$

$$\begin{aligned} O'_0 &= \frac{p_r}{2\Delta p}\left[\frac{18\tau_d}{T}\log_2\left(\frac{\tau_d}{T}\right) + \frac{34\tau_d}{T}\right] \\ &= \frac{0.098}{2 \times 0.002} \times \left[\frac{18 \times 51.2}{0.2} \times \log_2\left(\frac{51.2}{0.2}\right) + \frac{34 \times 51.2}{0.2}\right] \\ &= 1116416 \end{aligned} \tag{77}$$

TABLE 3. Mean RMSE of Doppler rate estimations with different methods; units are in *g*.

Methods	Case 1	Case 2	Case 3	Case 4
Proposed, with $\Delta p = \frac{\Delta p_o}{2}$	7.190	8.127	3.174	1.799
DFRFT with $\Delta p = 0.001$	7.091	6.739	2.165	1.415
DFRFT with $\Delta p = 0.002$	9.410	6.689	2.433	2.117
DFRFT with $\Delta p = 0.004$	15.392	9.341	2.925	3.561
DFRFT with $\Delta p = 0.006$	20.604	11.785	3.458	5.351
DFRFT with $\Delta p = \frac{\Delta p_o}{2}$	24.615	24.348	6.341	6.188

where O_0 denotes upper bound of the computational complexity with proposed algorithms, while O'_0 represents the lower bound of it. The computational improvement for proposed algorithm can be approximated as

$$\begin{aligned} r &= \frac{O_0 - O_p}{O_p} = \frac{2232832 - \left[410112 + 21 \cdot \Theta\left(2^3\right)\right]}{410112 + 21 \cdot \Theta\left(2^3\right)} \\ &\approx 444.44\% \\ r' &= \frac{O'_0 - O_p}{O_p} = \frac{1116416 - \left[410112 + 21 \cdot \Theta\left(2^3\right)\right]}{410112 + 21 \cdot \Theta\left(2^3\right)} \\ &\approx 172.22\% \end{aligned} \tag{78}$$

where r denotes the percentage of maximum improvement, while r' stands for the percentage of minimum improvement. Since $21\Theta\left(2^3\right)$ is very small when it is compared with the total complexity, it is omitted in the computations. Therefore, it can be concluded that the performance of the proposed novel Doppler rate estimator is much better than the original digital FRFT, and the improvements are around $172.22\% - 444.44\%$ for Case 4.

The summaries for the analysis of the computational complexities and the improvements with all cases mentioned in Table 2 are listed in Table 4, where the computational complexity related to the NLS estimation process is very small so that it is omitted in the calculation as mentioned earlier.

VIII. ANALYSIS AND DISCUSSION

In this section, some analysis and discussions based on simulation results will be presented. Some arguments of proposed algorithms on comparisons with previous works will be also provided. At last, the achievements and significance of our works would be illustrated.

A. ESTIMATION ACCURACY

Some conclusions can be drawn through Fig. 10 and Fig. 11. On the one hand, the simulation results in Case 3 and Case 4 with proposed algorithms are very similar to the ones estimated by the DFRFT implementation with a fine order bin size. However, the computational cost of proposed algorithms is much lower than the DFRFT with the fine bin size. So, it can be generally concluded that the computation efficiency has been improved. Some more rigorous analysis for the

TABLE 4. Computational complexity performance of proposed Doppler rate estimator.

Case	O_p	Better than	Worse than	r'	r
1	227840	DFRFT with $\Delta p = 0.002$	DFRFT with $\Delta p = 0.001$	110.00%	320.00%
2	102400	DFRFT with $\Delta p = 0.004$	DFRFT with $\Delta p = 0.002$	110.00%	320.00%
3	184320	DFRFT with $\Delta p = 0.006$	DFRFT with $\Delta p = 0.004$	81.48%	172.22%
4	410112	DFRFT with $\Delta p = 0.002$	DFRFT with $\Delta p = 0.001$	172.22%	444.44%

dependence of the estimation accuracy and computational complexity on the FRFT order search rate will be provided in Section VIII-B.

On the other hand, based on the results illustrated in Fig. 10, Fig. 11, Fig. 12, and Fig. 13, as well as the computational cost, O_p, listed in Table 4, proposed algorithms in the case with higher computational complexity can offer higher estimation accuracy. Since O_{nls} is so small when it is compared with O_p as mentioned earlier, it is omitted in the given results.

As shown in Fig. 13, the estimation accuracy of the Doppler rate with the ordinary DFRFT is highly influenced by the determined FRFT order bin, Δp. The narrower the FRFT order bin is, the more accurate estimations the DFRFT can provide. The estimation accuracies for the Doppler shift in Case 4 are higher than the accuracy results in Case 3, and proposed algorithms in Case 2 perform slightly better than the results in Case 1, as illustrated in Fig. 14. Besides, Doppler shift estimations in both Case 3 and Case 4 are evidently superior to the estimation results in Case 1 and Case 2. Secondly, when the longer dwell time is used for DFRFT implementation, both accurate Doppler rate and Doppler shift results can be estimated in a more accurate way. Besides, the sampling interval would theoretically make a slight difference on the final estimation results. If the dwell time is fixed, more promising estimation results in terms of the Doppler rate can be offered when a larger sampling interval in frequency domain is determined referring to (18), (37), (54), and (69). Therefore, the performance of the Doppler shift estimation is highly related to the dwell time but not so dependent on the level of the computational complexity. Nevertheless, both of these two factors play a significant role to influence the accuracy of the Doppler rate estimations. In reality, when the chosen FRFT order bin is narrower, the final results will be more possible to be influenced by the noise random error instead of the frequency sampling interval. Then, the Doppler shift estimation is dependent on both frequency resolution and the Doppler rate estimation accuracy as mentioned in (19), (36), (57), and (70). Thirdly, since different settings in terms of dwell time and sampling interval are used to verify our proposed algorithms, it can be proved from the estimation results that the proposed algorithm can perform much better with the determined optimal FRFT order bin than the results obtained from the ordinary DFRFT with the same FRFT order bin size.

Finally, the estimation accuracies of Doppler rate with proposed algorithms are compared with the ones estimated from the DFRFT method when the same FRFT order bin size is used. Referring to Table 3, the results of the first row and the sixth row should be contained in comparison. Based on the computation process of (78), similarly, the percentages of the improvement for Case 1 to 4 are calculated as 242.35%, 199.59%, 99.78%, and 243.96%, respectively. So, the estimation accuracy has largely been improved by proposed algorithms when compared with the ordinary DFRFT.

B. COMPUTATIONAL COMPLEXITY

Referring to the data in Table 4, the computation efficiency for all involved cases have significantly been improved with proposed algorithms. The improvement performs worst in Case 3 which is within a minimum improved percentage of 81.48%, while the estimation results in Case 4 benefit most from proposed algorithms, and the computational complexity can be reduced by minimum 172.22%. However, the real improvements will be more than the minimum value referring to the means of the RMSE listed in Table 3. In conclusion, it can be proved that the proposed novel Doppler rate estimator as described in Algorithm 2 and Algorithm 3 has the ability to highly improve the computation efficiency based on the DFRFT implementation.

C. COMPARISONS WITH PREVIOUS ALGORITHMS

There are some other algorithms reported in previous works being used to increase the computation efficiency. For instance, a two-dimensional (2D) neighbor search approach is proposed to reduce the search range of the FRFT order [33]. The brief idea for this algorithm will be subsequently described. Once an initial acceleration or Doppler rate is detected with the digital FRFT [15], the search range in terms of the FRFT order bin related to the following Doppler rate estimations can be narrowed with (19), and more detailed explanations can be read in [33]. However, there is lack of explanation why the FRFT order bin is set to 0.001 in their work. If an over small search bin is used in the digital implementation, the computation complexity can be seriously increased [32] and the fact is not allowed to occur in the real-time implementation. On the other hand, it can be noticed that the parameter setting for the digital FRFT implementation in [33] is identical to Case 4 as shown in Table 2 in our research. Estimation results based on the algorithms of the

DFRFT implementation in [33] and this work are corresponded to DFRFT: $\Delta p = 0.001$ and Proposed: $\Delta p = \frac{\Delta p_o}{2}$, respectively. Therefore, it can be concluded that proposed algorithms outperform the 2D neighbor search approach introduced in [33] based on previous analysis, and the 2D neighbor search can even be improved with a proper FRFT order bin calculated through Algorithm 1 in this work.

A maximum-amplitude-based coarse-to-fine (MACF) algorithm is also proposed in previous work [36] to shrink the FRFT search range as much as possible. However, some limitations could not be ignored when this algorithm will be applied to different types of signals. The acquisition process for dynamic and weak GNSS signals based on the DFRFT with the MACF will be taken as an example here. If parameter setting is initially determined with an inappropriate coarse FRFT order bin for the signal acquisition in a weak and dynamic situation, the FRFT amplitude peak of the real signal will be buried with the noise at a very high possibility. More DFRFT implementations have to be contained in the computation to confirm a correct estimation, and extra computational complexities would be added in this situation. Algorithm 1 is presented in this work to deal with this given issue and a maximum FRFT order bin can be finally constrained within a reasonable range. On the other hand, the maximum and minimum FRFT order bins are chosen as 0.1 and 0.001, respectively, through the search procedure with the MACF algorithm. There is no explanation why these values are decided here. Since an appropriate FRFT order bin is highly related to the sampling interval T, dwell time τ_d, and the dynamics of the incoming signal as described in Algorithm 1, it is possible that the optimal order bin is larger than 0.1 and less than 0.001. It means that the MACF is not globally applicable for various types of the signal processing. However, proposed algorithms have the potential scope of dealing with different types of LFM signals. Furthermore, extra DFRFT implementations, with respect to the change of the range from beginning coarse search order bin to the final fine search order bin, must be contained based on the MACF algorithm to find out an optimal FRFT order bin. Nevertheless, proposed Algorithm 1 is a brute force tool to find out the optimal FRFT order bin without any extra DFRFT implementations. At last, the final accurate estimation based on the MACF algorithm is dependent on a fine FRFT order bin, i.e., 0.001, as well after the coarse-to-fine search procedure. As mentioned earlier, a small order bin can highly increase the computational complexity of the DFRFT. However, proposed Algorithm 2 and Algorithm 3 provide a way to offer accurate estimations based on the DFRFT with a possibly maximum FRFT order bin.

An algorithm which is called as minimum norm method (MNM) [35] is also investigated by researchers to uncover the compact FRFT domain by searching the optimal FRFT order or angle that minimizes its ℓ_1-norm instead of the maximum amplitude as an improved version of the MACF method [36]. Simulations results demonstrate that the MNM performs better than the MACF method in terms of the number of significant amplitudes (NSA) and the ℓ_1-norm. The MNM and the MACF which are both followed with the coarse-to-fine search approach for the DFRFT hold the same computational cost whose total number of the DFRFT (NDFRFT) implementations is given by [35], [36]

$$N_{ref} = \left(\frac{p_r}{\Delta p_i} + 1\right) + \left(\lambda^{-1} + 1\right) \times \left\lceil \log_2 \left(\frac{\frac{\Delta p_i}{\varepsilon}}{\lambda^{-1}} \right) \right\rceil \quad (79)$$

where $\lceil \cdot \rceil$ denotes the ceiling function; Δp_i stands for the initial equidistant pieces in terms of the FRFT order bin; λ represents a variable parameter adjusting the order bin size for each loop implementation; ε provides a priori lower bound which is expected to quit the loop running at the last step. More detailed descriptions for (79) can be referred to [35] and [36]. On the other hand, according to (71), (73), (74), and (75), the total NDFRFTs for proposed algorithms can be generally attained as

$$N_p = \frac{p_r}{\Delta p_o} + 2 \quad (80)$$

It can be noticed that the performance of the MNM and the MACF method is highly related to the selection of three parameters, i.e., Δp_i, λ, and ε. As reported in [35], the coarse-to-fine approach is totally possible to fail to detect the global minimum with improper parameter settings. However, how to theoretically decide these parameters has seldom been mentioned in previous researches. In this case, the order bin has to be determined with a size as small as possible to guarantee the detection probability of the global minimum as high as possible [35], [36]. So, the order bin will usually be much smaller than the value it is expected to be to tolerate the uncertainty caused by the ambiguous settings with respect to the DFRFT as provided with (79) and corresponding discussions. The fast search algorithm of the DFRFT for the practical applications can be dramatically limited due to the narrow order bin size. In this research, we have presented some solutions to deal with this issue. For example, the DFRFT gain has been modeled with (33) in our work, the power loss of the global minimum has access to be constrained with the value of maximum 6 dB when it is compared with the estimation with a perfect match in the acquisition as provided with (38). Under this circumstance, the NDFRFT of the proposed algorithms is given by (80) which are only dependent on Δp_o instead of Δp_i, λ, and ε, when compared with (79). Again, Δp_o can be computed with proposed Algorithm 1 so that the FRFT order bin is finally fixed and it is also considered to be the maximum or optimal bin size. In a word, the proposed algorithms in this work manage to cover a significant gap related to the DFRFT as mentioned in [35].

Although, the optimal FRFT order bin size has been determined, but it cannot be used to confirm a high accuracy of the Doppler rate estimation. The order bin has to become smaller to improve the estimation performance and the computational burden is accordingly added. The proposed Algorithm 2 and

Algorithm 3 are proposed to provide a high estimation accuracy of the Doppler rate without narrowing the order bin size. In this way, only very small computational complexity will be extra added, i.e., $O_{nls} + O_2$. Otherwise, a higher computational cost would be taken with the DFRFT implementation to achieve a similarly high-precision solution if the proposed algorithms are not used as summarized in Table 3. In conclusion, the computational cost can be largely reduced with the proposed Algorithm 2 and Algorithm 3. In other words, the computational efficiency has been significantly improved as summarized in Table 4.

In addition, according to the earlier analysis and discussions, the coarse-to-fine search strategy is frequently used to confirm a fast DFRFT implementation. More detailed introduction for this algorithm can be referred to [36]. A loop iteration process based on the DFRFT implementation with varying FRFT orders and order bin sizes is the key idea for the coarse-to-fine algorithm. However, the first loop for the DFRFT implementation is dependent on the very ambiguous and coarse initial FRFT order range and search order bin. If these two parameters are determined with inappropriate values in the beginning, the estimation will be hard to be detected with the DFRFT at the first loop iteration, or the acquired estimation will be far from the real value. In this situation, more loop iterations have to be carried out to search for an accurate estimation as far as possible, so that the computational cost will be increased. Proposed algorithms, which provide novel ideas to compute an optimal order bin, i.e., Algorithm 1, and present a novel and fast Doppler rate estimator, i.e., Algorithm 2 and Algorithm 3, can largely speed up the DFRFT implementation in the first loop iteration according to the results listed in Table 3 and Table 4. Then, the coarse-to-fine search strategy will be certainly improved with proposed novel ideas. However, this research is not our main contribution in this work and it might be done in the future work.

D. ACHIEVEMENTS AND SIGNIFICANCE

Some achievements have been realized in this paper. According to the simulation results and comparisons between proposed algorithms and other previous algorithms, i.e., the 2D neighbor search approach [33], the MACF [36], and the MNM [35], it can be concluded that the proposed Algorithm 1, Algorithm 2, and Algorithm 3 are very efficient methods to improve the performances of the DFRFT implementation on both computational efficiency and estimation accuracy in terms of the acquisition process of the high-dynamic GNSS signal.

On the other hand, the significance of our work can be subsequently summarized. At first, an important issue which is reported in [35] have been solved as mentioned in Section VIII-C, i.e., the maximum power loss of the global minimum can be computed and a more simplified fast algorithm for the DFRFT is finally proposed. Besides, the estimation accuracy in terms of the Doppler rate based on the DFRFT can be improved without speeding up the sweeping rate of the FRFT order dimension and the computational complexity can be largely reduced. The fact can help the DFRFT become more promising to be applied in practical applications. In other words, the proposed algorithms can perform more efficiently on the fast DFRFT implementation process. In addition, they also have the scope of processing different types of LFM signals besides of the dynamic GNSS signal.

IX. CONCLUSION

The FRFT order search dimension is highly related to the implementation efficiency of the digital FRFT process. The Doppler rate of high-dynamic GNSS signal can be efficiently estimated with the FRFT algorithm when the FRFT order is accurately determined. In this research, an algorithm is firstly proposed is compute the optimal FRFT order bin as described in Algorithm 1; then, a novel Doppler rate estimator with the optimal FRFT order bin are introduced to offer an accurate Doppler rate estimation as mentioned in Algorithm 2; finally, an alternate search procedure is simultaneously proposed to reduce the singular estimations with the NLS method and corresponding contents are given in Algorithm 3. Simulations with proposed algorithms are carried out for four different cases with high-dynamic GPS L1 C/A signal as listed in Table 1 and Table 2. The estimation accuracy performances of Doppler shift and Doppler rate are evaluated. Then, the computational complexity of proposed algorithms are also computed in details. It can be proved that the computation efficiency has been significantly improved with proposed algorithms as well as the estimation accuracy has been largely increased. Proposed algorithms based on an optimal order bin size defined in this work can be deemed as one novel fast DFRFT algorithm which has seldom been researched in previous papers. Moreover, the proposed technique is an improvement of the FRFT algorithm itself, the scope of application for this technique is not limited. The mentioned scales can be adjusted flexibly for other types of LFM-signal, so it can be applied to other types of signal in the future.

APPENDIX

A. ABBREVIATIONS

The abbreviations used in this paper are listed in Table 5.

B. DERIVATIONS FOR THE THEORETICAL FRFT GAIN

The time delay error under high dynamics can be derived as

$$\Delta\tau_n = \frac{\bar{\omega}(n)}{2\pi f_r} nT \tag{81}$$

where subscript n denotes the index of discrete samples; $\bar{\omega}(n)$ is given by (8). Taking GPS L1 C/A signal into consideration in this research, the ACF of the spreading code during each

TABLE 5. List of abbreviations.

Abbreviation	Definition
ACF	auto-correlation function
A-GNSS	assisted global navigation satellite system
C/N_0	carrier-to-noise ratio density
DFRFT	digital fractional Fourier transform
FRFD	fractional Fourier domain
FRFT	fractional Fourier transform
FT	Fourier transform
GNSS	global navigation satellite system
GPS	global positioning system
IF	intermediate frequency
JPL	Jet Propulsion Laboratory
LB	lower bound
LFM	linear frequency modulation
MACF	maximum-amplitude-based coarse-to-fine
MNM	minimum norm method
NASA	National Aeronautics and Space Administration
NCO	numerically controlled oscillator
NDFRFT	number of the digital fraction Fourier transform
NLS	non-linear least square
NSA	number of significant amplitudes
RMSE	root-mean-square error
STD	standard deviation
2D	two-dimensional

sampling interval can be approximated as

$$R(\Delta\tau_n) = \begin{cases} 1 - \dfrac{\Delta\tau_n}{T_c}, & \Delta\tau_n \geq 0 \\ 1 + \dfrac{\Delta\tau_n}{T_c}, & \Delta\tau_n < 0 \end{cases} \tag{82}$$

Accordingly, if $\Delta\tau_n \geq 0$, R_Σ accounting for (20) can be derived as

$$\begin{aligned} R_\Sigma &\approx \frac{1}{N}\sum_{n=1}^{N}\left\{1 - \frac{\left[\Delta f n T + \frac{\mu}{2}(nT)^2\right]}{f_r T_c}\right\} \\ &= 1 - \frac{1}{N f_r T_c}\left\{\sum_{n=1}^{N}\left[\Delta f n T + \frac{\mu}{2}(nT)^2\right]\right\} \\ &= 1 - \frac{1}{N f_r T_c}\left\{\Delta f T \frac{(1+N)N}{2} + \frac{\mu T^2}{2}\frac{N(N+1)(2N+1)}{6}\right\} \\ &= 1 - \frac{1}{N f_r T_c}\left\{\frac{\left(N+N^2\right)\Delta f T}{2} + \frac{\left(2N^3+3N^2+N\right)\mu T^2}{12}\right\} \\ &= 1 - \frac{(1+N)\Delta f T}{2 f_r T_c} - \frac{\left(2N^2+3N+1\right)\mu T^2}{12 f_r T_c} \end{aligned} \tag{83}$$

Finally, given

$$R_\Sigma \approx \begin{cases} 1 - \dfrac{(1+N)\Delta f T}{2 f_r T_c} - \dfrac{\left(2N^2+3N+1\right)\mu T^2}{12 f_r T_c}, \\ \quad \Delta\tau_n \geq 0 \\ 1 + \dfrac{(1+N)\Delta f T}{2 f_r T_c} + \dfrac{\left(2N^2+3N+1\right)\mu T^2}{12 f_r T_c}, \\ \quad \Delta\tau_n < 0 \end{cases} \tag{84}$$

According to Euler's formula, given

$$\begin{aligned} sinc(\varphi_t) &= \frac{\sin\pi\varphi_t}{\pi\varphi_t} = \prod_{n=1}^{\infty}\left(1 - \frac{{\varphi_t}^2}{n^2}\right) \\ &\approx \left(1 - \frac{{\varphi_t}^2}{1^2}\right)\left(1 - \frac{{\varphi_t}^2}{2^2}\right) \\ &= 1 - {\varphi_t}^2 - \frac{{\varphi_t}^2}{4} + \frac{{\varphi_t}^4}{4} \\ &= 1 - \frac{5}{4}{\varphi_t}^2 + \frac{1}{4}{\varphi_t}^4 \end{aligned} \tag{85}$$

with

$$\varphi_t = \Delta f T + \frac{\mu}{2}Tt \tag{86}$$

Next, the absolute value of the integration with (85) can be derived as

$$\begin{aligned} &\left|\int_0^{NT} sinc\left(\Delta f T + \frac{\mu}{2}Tt\right)dt\right| \\ &= \left|\int_0^{NT} sinc(\varphi_t)\,dt\right| \\ &\approx \left|\int_0^{NT}\left(1 - \frac{5}{4}{\varphi_t}^2 + \frac{1}{4}{\varphi_t}^4\right)dt\right| \\ &= \left|NT - \int_0^{nT}\left(\frac{5}{4}{\varphi_t}^2\right)dt + \int_0^{nT}\left(\frac{1}{4}{\varphi_t}^4\right)dt\right| \\ &= \left|\begin{matrix} NT \\ +\int_0^{NT}\left\{\begin{matrix} \left[\frac{1}{4}(\Delta f T)^2\left((\Delta f T)^2 - 5\right)\right] \\ +\left[\frac{1}{4}\mu T\left(\Delta f T\right)\left(2(\Delta f T)^2 - 5\right)\right]t \\ +\left[\frac{1}{16}\mu^2 T^2\left(6(\Delta f T)^2 - 5\right)\right]t^2 \\ +\frac{1}{8}\Delta f\mu^3 T^4 t^3 + \frac{1}{64}\mu^4 T^4 t^4 \end{matrix}\right\}dt \end{matrix}\right| \end{aligned} \tag{87}$$

Supposing that $\varphi_0 = \Delta f T$, so,

$$\begin{aligned} \kappa_1^f &= \frac{1}{NT}\left|\int_0^{NT} sinc(\varphi_t)\,dt\right| \\ &= \frac{1}{NT}\left|\begin{matrix} NT \\ +\int_0^{NT}\left\{\begin{matrix} \left[\frac{1}{4}{\varphi_0}^2\left({\varphi_0}^2 - 5\right)\right] \\ +\left[\frac{1}{4}\mu T\varphi_0\left(2{\varphi_0}^2 - 5\right)\right]t \\ +\left[\frac{1}{16}\mu^2 T^2\left(6{\varphi_0}^2 - 5\right)\right]t^2 \\ +\frac{1}{8}\mu^3 T^3\varphi_0 t^3 + \frac{1}{64}\mu^4 T^4 t^4 \end{matrix}\right\}dt \end{matrix}\right| \end{aligned}$$

$$
\begin{aligned}
&= \left| \begin{array}{l} \left[\frac{1}{4}{\varphi_0}^2\left({\varphi_0}^2-5\right)+1\right] \\ +\left[\frac{1}{8}\mu T\varphi_0\left(2{\varphi_0}^2-5\right)\right]NT \\ +\left[\frac{1}{48}\mu^2T^2\left(6{\varphi_0}^2-5\right)\right]N^2T^2 \\ +\frac{1}{32}\mu^3\varphi_0N^3T^6+\frac{1}{320}\mu^4N^4T^8 \end{array} \right| \\
&= 1+\frac{{\varphi_0}^2\left({\varphi_0}^2-5\right)}{4}+\frac{\varphi_0\left(2{\varphi_0}^2-5\right)\mu NT^2}{8} \\
&\quad +\frac{\left(6{\varphi_0}^2-5\right)\mu^2N^2T^4}{48}+\frac{\varphi_0\mu^3N^3T^6}{32}+\frac{\mu^4N^4T^8}{320}
\end{aligned} \tag{88}
$$

κ_2^f can be derived as

$$
\begin{aligned}
\kappa_2^f &= \left|\frac{1}{NT}\int_0^{NT}\exp\left(j2\pi\delta ut\right)dt\right| \\
&= \left|\frac{1}{NT}\frac{1}{j2\pi\delta u}\exp\left(j2\pi\delta ut\right)|_0^{NT}\right| \\
&= \left|\frac{1}{NT}\frac{1}{j2\pi\delta u}\left[\exp\left(j2\pi\delta uNT\right)-1\right]\right| \\
&= \left|\begin{array}{l}\frac{1}{\pi\delta uNT}\exp\left(j\pi\delta uNT\right) \\ \times\frac{\exp\left(j\pi\delta unT\right)-\exp\left(-j\pi\delta unT\right)}{2j}\end{array}\right| \\
&= \left|\frac{1}{\pi\delta uNT}\sin\left(\pi\delta uNT\right)\right| = \left|sinc\left(\delta unT\right)\right| \\
&= sinc\left(\delta unT\right)
\end{aligned} \tag{89}
$$

C. DERIVATIONS FOR THE OPTIMAL FRFT ORDER BIN

According to (38), given

$$
10\lg\left[\left(G_R\right)^2\right] \geq -6 \Rightarrow G_R \geq \gamma \tag{90}
$$

Then, Doppler rate resolution is given by (37), and, again, it can be derived as follow

$$
\begin{aligned}
&\delta\mu_R \\
&= \left|\bar{\mu}-\left(-\frac{\cot\left(\bar{\alpha}+\frac{\pi}{4}\Delta p\right)}{NT^2}\right)\right|+\left|\bar{\mu}-\left(-\frac{\cot\left(\bar{\alpha}-\frac{\pi}{4}\Delta p\right)}{NT^2}\right)\right| \\
&= \left|\bar{\mu}+\frac{\cot\left(\bar{\alpha}+\frac{\pi}{4}\Delta p\right)}{NT^2}\right|+\left|\bar{\mu}+\frac{\cot\left(\bar{\alpha}-\frac{\pi}{4}\Delta p\right)}{NT^2}\right|
\end{aligned} \tag{91}
$$

Since Δp is narrow enough, it can be approximated as

$$
\frac{\delta\mu_R}{2} \approx \left|\bar{\mu}+\frac{\cot\left(\bar{\alpha}+\frac{\pi}{4}\Delta p\right)}{NT^2}\right| \approx \left|\bar{\mu}+\frac{\cot\left(\bar{\alpha}-\frac{\pi}{4}\Delta p\right)}{NT^2}\right| \tag{92}
$$

where $\bar{\mu}=-\frac{\cot\bar{\alpha}}{NT^2}$. Next, substitute (33) to (90), given

$$
R_\Sigma\kappa_1^f\kappa_2^fC_\alpha\left(1-0.02{r_2}^2-0.03{r_2}^4\right) \geq \gamma \tag{93}
$$

where r_2 is provided by (27) which can be assumed as an unknown variable here. Equation (93) can be also transferred to the form as follow

$$
{r_2}^4+B{r_2}^2+C \leq 0 \tag{94}
$$

where B and C are given by (41); γ is set to 0.5; C_α is approximated as $\frac{1}{\sqrt{|\sin\bar{\alpha}|}}$. In order to work out the solution of (94), based on mathematical theorems, it should satisfy

$$
0 \leq r_2 \leq \sqrt{\frac{-B+\sqrt{\Delta}}{2}} \tag{95}
$$

Again, known that

$$
r_2 = \frac{\sqrt{\pi\delta\mu}NT}{2} = \frac{\sqrt{\pi\frac{\delta\mu_R}{2}}NT}{2} \tag{96}
$$

Finally, it can be derived as

$$
\begin{aligned}
&\frac{\sqrt{\pi}NT\sqrt{\frac{\delta\mu_R}{2}}}{2} \leq \sqrt{\frac{-B+\sqrt{\Delta}}{2}} \\
&\Rightarrow \frac{\delta\mu_R}{2} \leq \frac{-2B+2\sqrt{\Delta}}{\pi N^2T^2} \\
&\Rightarrow \frac{\cot\left(\bar{\alpha}+\frac{\pi}{4}\Delta p\right)}{NT^2} \geq \frac{2B-2\sqrt{\Delta}}{\pi N^2T^2}-\bar{\mu} \\
&\Rightarrow 0<\Delta p \leq \frac{4}{\pi}\left\{cot^{-1}\left[\frac{2B-2\sqrt{\Delta}}{\pi N}-\bar{\mu}NT^2\right]-\bar{\alpha}\right\} \\
&\Rightarrow 0<\Delta p \leq \frac{4}{\pi}\left\{cot^{-1}\left[-2D-\bar{\mu}NT^2\right]-\bar{\alpha}\right\}
\end{aligned} \tag{97}
$$

with

$$
D = \frac{-B+\sqrt{\Delta}}{\pi N} \tag{98}
$$

D. DERIVATIONS FOR PROPOSED DOPPLER RATE ESTIMATOR BASED ON NON-LINEAR LEAST SQUARE METHOD

Substituting (25) and (30) to (45), the loss function can be finally derived as follow

$$
\begin{aligned}
J\left(\theta\right) &= \left|\left|X\left(p,u|\,p=\zeta^{-1}\left(\mu\right),u=f^{-1}\left(\delta u\right)\right)\right|-\tilde{P}\right|^2 \\
&= \left|R_\Sigma\kappa_1^fC_\alpha sinc\left(\delta uNT\right)\left(1-0.02s_{\delta\mu}-0.03s_{\delta\mu}^2\right)-\tilde{P}\right|^2 \\
&= \left(R_\Sigma\kappa_1^fC_\alpha\right)^2sinc^2\left(\delta uNT\right)\left(1-0.02s_{\delta\mu}-0.03s_{\delta\mu}^2\right)^2 \\
&\quad -2\tilde{P}R_\Sigma\kappa_1^fC_\alpha sinc\left(\delta uNT\right)\left(1-0.02s_{\delta\mu}-0.03s_{\delta\mu}^2\right) \\
&\quad +\tilde{P}^2
\end{aligned} \tag{99}
$$

with

$$
\begin{cases}
\delta\mu = \left|\zeta\left(p\right)-\mu\right| \\
s_{\delta\mu} = \frac{\pi}{4}\delta\mu N^2T^2 \\
\varphi_{\delta u} = \delta uNT
\end{cases} \tag{100}
$$

Besides, according to (85), it can be obtained as

$$
sinc\left(\varphi_{\delta u}\right) \approx 1-\frac{5}{4}{\varphi_{\delta u}}^2+\frac{1}{4}{\varphi_{\delta u}}^4 \tag{101}
$$

Noticing that when the signal is detected with digital FRFT implementation as given by (44), p' and u' currently can both be assumed as the quasi-real values. This fact lead to the consequence that $\varphi_{\delta u}$ is very close to zero. Higher order terms of Euler's formula can be removed and $sinc\,(\varphi_{\delta u})$ can, accordingly, approximated as the form of (101). So, the partial derivative of (101) satisfies

$$\begin{aligned}\frac{\partial sinc\,(\delta u \cdot NT)}{\partial \delta u} &= \frac{\partial\left[1-\frac{5}{4}{\varphi_{\delta u}}^2+\frac{1}{4}{\varphi_{\delta u}}^4\right]}{\partial \delta u}\\ &= -\frac{5}{2}\varphi_{\delta u} NT+{\varphi_{\delta u}}^3 NT \end{aligned} \tag{102}$$

Furthermore, the corresponding partial derivatives of (47) can be given as follows, i.e.,

$$\begin{aligned}\frac{\partial J\,(\theta,\xi)}{\partial \delta u} &= 2R_\Sigma \kappa_1^f C_\alpha\left(1-0.02s_{\delta\mu}-0.03s_{\delta\mu}^2\right)\\ &\quad\times\left({\varphi_{\delta u}}^3-\frac{5}{2}\varphi_{\delta u}\right)NT\\ &\quad\times\left[\begin{array}{l}R_\Sigma\kappa_1^f C_\alpha\\ \times\left(1-0.02s_{\delta\mu}-0.03s_{\delta\mu}^2\right)\\ \times sinc\,(\delta u NT)\\ -\tilde{P}\end{array}\right]\end{aligned} \tag{103}$$

and

$$\begin{aligned}\frac{\partial J\,(\theta,\xi)}{\partial \delta \mu} &= 2\cdot\left(R_\Sigma\kappa_1^f C_\alpha\right)^2 sinc^2\,(\delta u\cdot NT)\\ &\quad\times\left(1-0.02s_{\delta\mu}-0.03s_{\delta\mu}^2\right)\\ &\quad\times\left(-0.02-0.06s_{\delta\mu}\right)\frac{\partial s_{\delta\mu}}{\partial\delta\mu}\\ &\quad-2\tilde{P}R_\Sigma\kappa_1^f C_\alpha sinc\,(\delta u\cdot NT)\\ &\quad\times\left(-0.02-0.06s_{\delta\mu}\right)\frac{\partial s_{\delta\mu}}{\partial\delta\mu}\end{aligned} \tag{104}$$

with

$$\frac{\partial s_{\delta\mu}}{\partial\delta\mu}=\frac{\pi}{4}N^2T^2 \tag{105}$$

Hence, the results can be given as follow

$$\begin{aligned}\frac{\partial J\,(\theta,\xi)}{\partial \delta u} &= 2R_\Sigma\kappa_1^f C_\alpha\times\left(1-0.02s_{\delta\mu}-0.03s_{\delta\mu}^2\right)\\ &\quad\times\left({\varphi_{\delta u}}^3-\frac{5}{2}\varphi_{\delta u}\right)NT\\ &\quad\times\left[\begin{array}{l}\left(R_\Sigma\kappa_1^f C_\alpha\right)sinc\,(\delta u NT)\\ \times\left(1-0.02s_{\delta\mu}-0.03s_{\delta\mu}^2\right)\\ -\tilde{P}\end{array}\right]\end{aligned} \tag{106}$$

$$\begin{aligned}\frac{\partial J\,(\theta,\xi)}{\partial \delta \mu} &= \pi N^2T^2R_\Sigma\kappa_1^f C_\alpha\\ &\quad\times sinc\,(\delta u NT)\left(-0.01-0.03s_{\delta\mu}\right)\\ &\quad\times\left[\begin{array}{l}\left(R_\Sigma\kappa_1^f C_\alpha\right)sinc\,(\delta u NT)\\ \times\left(1-0.02s_{\delta\mu}-0.03s_{\delta\mu}^2\right)\\ -\tilde{P}\end{array}\right]\end{aligned} \tag{107}$$

REFERENCES

[1] N. Gao and L. Zhao, "An integrated land vehicle navigation system based on context awareness," *GPS Solutions*, vol. 20, no. 3, pp. 509–524, 2016.

[2] G. MacGougan *et al.*, "Performance analysis of a stand-alone high-sensitivity receiver," *GPS Solutions*, vol. 6, no. 3, pp. 179–195, 2002.

[3] T. Ren and M. G. Petovello, "A stand-alone approach for high-sensitivity gnss receivers in signal-challenged environment," *IEEE Trans. Aerosp. Electron. Syst.*, vol. 53, no. 5, pp. 2438–2448, Oct. 2017.

[4] S. Chen, Y. Gao, and T. Lin, "Effect and mitigation of oscillator vibration-induced phase noise on carrier phase tracking," *GPS Solutions*, vol. 21, no. 4, pp. 1515–1524, 2017.

[5] S. Chen and Y. Gao, "Improvement of carrier phase tracking in high dynamics conditions using an adaptive joint vector tracking architecture," *GPS Solutions*, vol. 23, no. 1, p. 15, 2019.

[6] H. Ruan, J. Li, L. Zhang, and T. Long, "Adaptive correlation space adjusted open-loop tracking approach for vehicle positioning with global navigation satellite system in urban areas," *Sensors*, vol. 15, no. 9, pp. 21581–21612, 2015.

[7] A. M. M. Kamel, "Context aware high dynamics GNSS-INS for interference mitigation," Ph.D. dissertation, Dept. Geomatics Eng., Univ. Calgary, Calgary, AB, Canada, 2011.

[8] T. S. Bruggemann, D. G. Greer, and R. A. Walker, "GPS fault detection with IMU and aircraft dynamics," *IEEE Trans. Aerosp. Electron. Syst.*, vol. 47, no. 1, pp. 305–316, Jan. 2011. [Online]. Available: http://ieeexplore.ieee.org/document/5705677/

[9] V. Capuano, C. Botteron, Y. Wang, J. Tian, J. Leclère, and P.-A. Farine, "GNSS/INS/Star tracker integrated navigation system for Earth-Moon transfer orbit," in *Proc. 27th Int. Tech. Meeting Satell. Division Inst. Navigat. (ION GNSS)*, vol. 2, 2014, pp. 1433–1447.

[10] V. Capuano, C. Botteron, J. Leclère, J. Tian, Y. Wang, and P. A. Farine, "Feasibility study of GNSS as navigation system to reach the Moon," *Acta Astronautica*, vol. 116, pp. 186–201, Nov./Dec. 2015. [Online]. Available: http://linkinghub.elsevier.com/retrieve/pii/S0094576515002520

[11] M. Manzano-Jurado *et al.*, "Use of weak GNSS signals in a mission to the Moon," in *Proc. IEEE 7th ESA Workshop Satellite Navigat. Technol. Eur. Workshop GNSS Signals Signal Process. (NAVITEC)*, Dec. 2014, pp. 1–8. [Online]. Available: http://ieeexplore.ieee.org/document/7045151/

[12] N. El-Sheimy, S. Nassar, and A. Noureldin, "Wavelet de-noising for IMU alignment," *IEEE Aerosp. Electron. Syst. Mag.*, vol. 19, no. 10, pp. 32–39, Oct. 2004.

[13] Y. Kubo, M. Nishiyama, and S. Fujioka, "Nonlinear filtering methods for the INS/GPS in-motion alignment and navigation," *Inf. Control*, vol. 2, no. 5, pp. 1137–1151, 2006.

[14] L. B. Almeida, "The fractional Fourier transform and time-frequency representations," *IEEE Trans. Signal Process.*, vol. 42, no. 11, pp. 3084–3091, Nov. 1994.

[15] H. M. Ozaktas, O. Arikan, M. A. Kutay, and G. Bozdagt, "Digital computation of the fractional Fourier transform," *IEEE Trans. Signal Process.*, vol. 44, no. 9, pp. 2141–2150, Sep. 1996.

[16] D. Gaglione *et al.*, "Waveform design for communicating radar systems using fractional Fourier transform," *Digit. Signal Process.*, vol. 80, pp. 57–69, Sep. 2018.

[17] N. Liu, R. Tao, R. Wang, Y. Deng, N. Li, and S. Zhao, "Signal reconstruction from recurrent samples in fractional Fourier domain and its application in multichannel SAR," *Signal Process.*, vol. 131, pp. 288–299, Feb. 2017.

[18] F. Pérez, B. Santhanam, R. Dunkel, and M. M. Hayat, "Clutter suppression via Hankel rank reduction for DFrFT-based vibrometry applied to SAR," *IEEE Geosci. Remote Sens. Lett.*, vol. 14, no. 11, pp. 2052–2056, Nov. 2017.

[19] X. Feng, Y.-N. Zhao, Z.-F. Zhao, and Z.-Q. Zhou, "Cognitive tracking waveform design based on multiple model interaction and measurement information fusion," *IEEE Access*, vol. 6, pp. 30680–30690, 2018.

[20] X. Chen, B. Chen, Y. Huang, Y. He, and J. Guan, "Space-range-Doppler focus-based low-observable moving target detection using frequency diverse array MIMO radar," *IEEE Access*, vol. 6, pp. 43892–43904, 2018.

[21] M. Gonzalez-Lee *et al.*, "Exploring the cross-correlation as a means for detecting digital watermarks and its reformulation into the fractional calculus framework," *IEEE Access*, vol. 6, pp. 71699–71718, 2018.

[22] M. H. Annaby, H. Ayad, M. A. Rushdi, and E. Nehary, "Difference operators and generalized discrete fractional transforms in signal and image processing," *Signal Process.*, vol. 151, pp. 1–18, Oct. 2018.

[23] X. Da *et al.*, "Embedding WFRFT signals into TDCS for secure communications," *IEEE Access*, vol. 6, pp. 54938–54951, 2018.

[24] L. Yang, P. Guo, A. Yang, and Y. Qiao, "Blind third-order dispersion estimation based on fractional Fourier transformation for coherent optical communication," *Opt. Laser Technol.*, vol. 99, pp. 86–90, Feb. 2018.
[25] X. Chen, Z. Liu, and X. Wei, "Fast FRFT-based algorithm for 3-D LFM source localization with uniform circular array," *IEEE Access*, vol. 6, pp. 2130–2135, 2018.
[26] J. Chen and J. Hu, "Detecting the spatial chirp signals by fractional Fourier lens with transformation materials," *Appl. Phys. A*, vol. 124, no. 2, p. 154, 2018.
[27] Y. Zhao, H. Yu, G. Wei, F. Ji, and F. Chen, "Parameter estimation of wideband underwater acoustic multipath channels based on fractional Fourier transform," *IEEE Trans. Signal Process.*, vol. 64, no. 20, pp. 5396–5408, Oct. 2016.
[28] X. Chen, J. Guan, N. Liu, and Y. He, "Maneuvering target detection via radon-fractional Fourier transform-based long-time coherent integration," *IEEE Trans. Signal Process.*, vol. 62, no. 4, pp. 939–953, Feb. 2014.
[29] B. B. Ibrahim and A. H. Aghvami, "Direct sequence spread spectrum matched filter acquisition in frequency-selective Rayleigh fading channels," *IEEE J. Sel. Areas Commun.*, vol. 12, no. 5, pp. 885–890, Jun. 1994.
[30] A. Polydoros and C. Weber, "A unified approach to serial search spread-spectrum code acquisition—Part I: General theory," *IEEE Trans. Commun.*, vol. COM-32, no. 5, pp. 542–549, May 1984.
[31] R. A. Stirling-Gallacher, A. P. Hulbert, and G. J. R. Povey, "A fast acquisition technique for a direct sequence spread spectrum signal in the presence of a large Doppler shift," in *Proc. IEEE 4th Int. Symp. Spread Spectr. Techn. Appl.*, vol. 1, Sep. 1996, pp. 156–160.
[32] Y. Luo, L. Zhang, and H. Ruan, "An acquisition algorithm based on FRFT for weak GNSS signals in a dynamic environment," *IEEE Commun. Lett.*, vol. 22, no. 6, pp. 1212–1215, Jun. 2018.
[33] X. Xia, J. Zhao, H. Long, G. Yang, J. Sun, and W. Yang, "Fractional Fourier transform-based unassisted tracking method for Global Navigation Satellite System signal carrier with high dynamics," *IET Radar, Sonar Navigat.*, vol. 10, no. 3, pp. 506–515, 2016.
[34] Y. Luo, L. Zhang, and N. El-Sheimy, "An improved DE-KFL for BOC signal tracking assisted by FRFT in a highly dynamic environment," in *Proc. IEEE/ION Position, Location Navigat. Symp. (PLANS)*, Apr. 2018, pp. 1525–1534.
[35] A. Serbes, "Compact fractional Fourier domains," *IEEE Signal Process. Lett.*, vol. 24, no. 4, pp. 427–431, Apr. 2017.
[36] L. Zheng and D. Shi, "Maximum amplitude method for estimating compact fractional Fourier domain," *IEEE Signal Process. Lett.*, vol. 17, no. 3, pp. 293–296, Mar. 2010.
[37] H. M. Ozaktas and M. A. Kutay, "The fractional Fourier transform," in *Proc. IEEE Eur. Control Conf. (ECC)*, Sep. 2001, pp. 1477–1483.
[38] T. Erseghe, P. Kraniauskas, and G. Carioraro, "Unified fractional Fourier transform and sampling theorem," *IEEE Trans. Signal Process.*, vol. 47, no. 12, pp. 3419–3423, Dec. 1999.
[39] E. D. Kaplan and C. Hegarty, *Understanding GPS: Principles and Applications*. Norwood, MA, USA: Artech House, 2005.
[40] J. Song, Y. Wang, and Y. Liu, "Iterative interpolation for parameter estimation of lfm signal based on fractional Fourier transform," *Circuits, Syst., Signal Process.*, vol. 32, no. 3, pp. 1489–1499, 2013.
[41] S. Hined and J. I. Statman, "High-dynamic GPS tracking," Jet Propuls. Lab., California Inst. Technol., Pasadena, CA, USA, Final Rep. NASA-CR-184868, 1988.
[42] P. J. G. Teunissen, "Nonlinear least squares," *Manuscripta Geodaetica*, vol. 15, no. 3, pp. 137–150, 1990.
[43] R. G. Brown and P. Y. C. Hwang, *Introduction to Random Signals and Applied Kalman Filtering With MATLAB Exercises*, 4th ed. Hoboken, NJ, USA: Wiley, 2012.
[44] F. van Diggelen, *A-GPS: Assisted GPS, GNSS, and SBAS*. Norwood, MA, USA: Artech House, 2009.
[45] S.-H. Kong and W. Nam, "A-GNSS sensitivity for parallel acquisition in asynchronous cellular networks," *IEEE Trans. Wireless Commun.*, vol. 9, no. 12, pp. 3770–3778, Dec. 2010. [Online]. Available: http://ieeexplore.ieee.org/document/5595725/
[46] F. Dovis, R. Lesca, G. Boiero, and G. Ghinamo, "A test-bed implementation of an acquisition system for indoor positioning," *GPS Solutions*, vol. 14, no. 3, pp. 241–253, 2010.
[47] J. W. Cheong, J. Wu, and A. Dempster, "Dichotomous search of coarse time error in collective detection for GPS signal acquisition," *GPS Solutions*, vol. 19, no. 1, pp. 61–72, 2014.
[48] P. S. Maybeck, *Stochastic Models, Estimation and Control* (Mathematics in Science and Engineering), vol. 3, New York, NY, USA: Academic, 1979.
[49] T. H. Cormen, C. E. Leiserson, R. L. Rivest, and C. Stein, *Introduction to Algorithms*. Cambridge, MA, USA: MIT Press, 2009.

YIRAN LUO received the B.S. degree in electronic information science and technology from Sichuan University, China, in 2014. She is currently pursuing the Ph.D. degree with the Department of Geomatics Engineering, University of Calgary, Canada, and with the School of Information and Electronics, Beijing Institute of Technology, China. Her research interests include GNSS signal processing, GNSS receiver design, GNSS/INS integration systems, multi-sensor integration, and autonomous vehicle navigation. She was a recipient of the Best Paper Award for China Satellite Navigation Conference, in 2017.

CHUNYANG YU received the Ph.D. degree in positioning, navigation, and wireless location from the University of Calgary, Canada, where she is currently a Postdoctoral Fellow with the Mobile Multi-Sensor Systems Research Group. Her research interests include inertial sensor-based navigation systems, specifically, pedestrian navigation system and autonomous vehicle navigation systems.

SHAOHUA CHEN received the M.Sc. degree in electrical engineering from the Beijing Institute of Technology, in 2012, and the Ph.D. degree from the Department of Geomatics Engineering, University of Calgary, where he is currently a Research Assistant. His research interests include GNSS receiver design, digital signal processing, and high precision positioning.

JIAN LI received the B.S. and Ph.D. degrees in electrical engineering from the Beijing Institute of Technology, China, in 2004 and 2009, respectively, where he is currently a Lecturer with the School of Information and Electronics. His research interests include GNSS baseband signal processing and GNSS receiver design.

HANG RUAN received the B.S. and Ph.D. degrees from the School of Information and Electronics, Beijing Institute of Technology, China, in 2011 and 2017, respectively. He is currently with the Beijing Institute of Radio Measurement, China. His research interests include signal processing, digital beamform, and GNSS software receiver.

NASER EL-SHEIMY is currently a Professor with the Department of Geomatics Engineering, University of Calgary. He is also the Founder and the CEO of Profound Positioning Inc. He has published two books, six book chapters, and over 450 papers in academic journals, conference, and workshop proceedings, in which he has received over 30 national and international paper awards. He supervised and graduated over 60 master's and Ph.D. students. His research interest includes geomatics multi-sensor systems, GPS/INS integration, and mobile mapping systems. He is a Fellow of the Canadian Academy of Engineering and the U.S. Institute of Navigation. He was a recipient of many national and international awards, including the ASTech Leadership in Alberta Technology Award and the Association of Professional Engineers, Geologists, and Geophysicists of Alberta Educational Excellence Award. He is also the Tier-I Canada Research Chair in Geomatics Multi-Sensor Systems.